Identification of a novel toxicophore in anti-cancer chemotherapeutics that targets mitochondrial respiratory complex I

Zoë A. Stephenson[1], Robert F. Harvey[1*], Kenneth R. Pryde[1*], Sarah Mistry[2], Rachel Hardy[1], Riccardo Serreli[3], Injae Chung[3], Timothy E. H. Allen[1], Mark Stoneley[1], Marion MacFarlane[1], Peter Fischer[2], Judy Hirst[±3], Barrie Kellam[±2], Anne E. Willis[±1]

1. MRC Toxicology Unit, University of Cambridge, Lancaster Rd, Leicester LE1 9HN
2. School of Pharmacy, Biodiscovery Institute, University of Nottingham, University Park, Nottingham NG2 7RD
3. MRC Mitochondrial Biology Unit, University of Cambridge, Cambridge CB2 0XY

Correspondence: Anne Willis aew80@mrc-tox.cam.ac.uk; barrie.kellam@nottingham.ac.uk; jh@mrc-mbu.cam.ac.uk

± Joint senior and corresponding authors

* Equal contribution

Abstract

Disruption of mitochondrial function selectively targets tumour cells that are dependent on oxidative phosphorylation. However, due to their high energy demands, cardiac cells are disproportionately targeted by mitochondrial toxins resulting in a loss of cardiac function. An analysis of the effects of mubritinib on cardiac cells showed that this drug did not inhibit HER2 as reported, but directly inhibits mitochondrial respiratory complex I, reducing cardiac-cell beat rate, with prolonged exposure resulting in cell death. We used a library of chemical variants of mubritinib and showed that modifying the 1H-1,2,3-triazole altered complex I inhibition, identifying the heterocyclic 1,3-nitrogen motif as the toxicophore. The same toxicophore is present in a second anti-cancer therapeutic carboxyamidotriazole (CAI) and we demonstrate that CAI also functions through complex I inhibition, mediated by the toxicophore. Complex I inhibition is directly linked to anti-cancer cell activity, with toxicophore modification ablating the desired effects of these compounds on cancer cell proliferation and apoptosis.

Introduction

The pharmaceutical industry must deliver safe and effective medicines while simultaneously limiting the costs associated with drug development, and a central part of this process is de-risking potential safety liabilities at an early stage [1]. In many cases, lack of mechanistic understanding about how compounds cause toxicity hampers predictions of adverse drug reactions (ADRs), and more information about the specific substructures of drug molecules that cause ADRs is required. Such information can then be used to populate machine learning algorithms to generate adverse outcome pathways (AOPs) that predict likely outcomes [2] from off-target toxicities and that can be used in early phase drug design [3].

It is widely accepted that disruption of mitochondrial function is a common cause of ADRs and it has been proposed that mitochondrial toxicity, which has a major role in idiosyncratic drug toxicity [4], is responsible for up to 50% of post-market drug withdrawals [5,6]. Mitochondrial toxins often have a differential effect on tissue function due to organ-specific variations in the mitochondrial proteome and its function [7]; primarily biosynthetic and metabolic in liver, and energy production in muscle [8, 9]. For example, cardiomyocytes, which have high energy requirements and are rich in mitochondria [10], are particularly sensitive to mitochondrial toxins that alter ATP production [11]. Mitochondria are central to many cell-wide processes so mitochondrial toxicity affects bioenergetics, metabolism, signalling and oxidative stress [12] in addition to impacting stemness, differentiation and apoptosis [13]. Due to these pleiotropic roles, “off-target” drug toxicity resulting in impairment of mitochondrial function can easily be misattributed to other targets and cellular processes.

Given the relative paucity of mechanistic knowledge relating specific drug substructures to ADRs we carried out a detailed chemical dissection of mubritinib, which was reported to act as a tyrosine kinase (HER2) inhibitor and which has been trialled as a treatment for a range of cancers [14, 15]. However, mubritinib has also been shown to affect energy status [16, 17], and it was recently demonstrated to have an "off-target" effect on mitochondrial function through inhibition of respiratory complex I in cells derived from patients with Acute Myeloid Leukaemia (AML), leading to a new therapeutic option [16].

Here, we show that mubritinib does not bind directly to HER2 and that its inhibitory effect on complex I negatively impacts on cardiomyocyte function, an important clinical consideration. Through the use of a focussed chemical library, we show that modifying the 1*H*-1,2,3-triazol-1-yl moiety present in mubritinib substantially alters both the inhibition of complex I and the toxicity to cardiomyocytes; identifying a heterocyclic 1,3-nitrogen motif as being key to its complex I inhibitory action. A search of chemical space was then undertaken for the same substructure, and led to the drug carboxyamidotriazole (CAI), which has also been trialled as an anti-cancer agent [17,18-20]. We show that, like mubritinib, CAI does not directly inhibit its reported target (calcium channels) and is also a potent complex I inhibitor. Furthermore, like mubritinib, chemically altering the triazole ring moiety ablated toxicity. In both cases we show that mitochondrial toxicity is directly linked to anti-cancer activity, as chemical manipulation of the toxicophoric heterocycle ablates the desired effects of both compounds on cancer-cell proliferation and apoptosis. Thus, we have identified a novel toxicophoric motif that is mechanistically linked to an adverse cardiac cell event. Our data demonstrate that caution must be taken when attributing a drug mechanism of action without detailed structure activity relationship (SAR) analysis, since inhibition of mitochondrial function has such cell-wide effects.

Results

Mubritinib is not a direct HER2 inhibitor, but instead inhibits ATP production in h9c2 cells and reduces beat rate in cardiomyocytes

Previous data have reported that mubritinib inhibits phosphorylation of HER2 in breast cancer cell lines that express high levels of this receptor [14]. Therefore, the HER2-overexpressing cell line, BT474, was treated with increasing doses of mubritinib and the effect on HER2 phosphorylation was analysed by Western blotting, with the specific HER2 inhibitor lapatinib [21] as a positive control (Figure 1A, Figure 1-figure supplement 1A). Surprisingly, there was only a small decrease in HER2 phosphorylation in the presence of mubritinib, in contrast to lapatinib. Furthermore, recent data have further shown that mubritinib, in common with known inhibitors of mitochondrial respiratory complex I [22], alters the phosphorylation status of proteins that sense changes in energy status and stimulate cellular proliferation, such as mTOR [23]. In agreement with these data, we show that treatment of cells with mubritinib (Figure 1B) alters the phosphorylation status of proteins downstream of the energy sensor AMPK (e.g. acetyl-CoA carboxylase) and impacts on mTOR signalling (e.g. phosphorylation of RPS6, Figure 1-figure supplement 1B). Moreover, similar effects were also observed with treatment by the known mitochondrial inhibitors, rotenone and antimycin A (Figure 1B and Figure 1-figure supplement 1Ci and ii). In contrast, lapatinib, which is a specific HER2 inhibitor, blocks signalling downstream from mTOR with minimal effect on ACC phosphorylation (Figure 1B, Figure 1-figure supplement 1Ci and ii), but a large effect on RPS6 (Figure 1-figure supplement 1Ci and ii). An inactive mubritinib analogue (compound **5**, see below) was used as a negative control. An *in vitro* tyrosine kinase activity assay was then carried out with increasing concentrations of

mubritinib, in which recombinant human HER2 was incubated with radioactively labelled ^{32}P-ATP. Mubritinib did not decrease ^{32}P incorporation, even at 10 μM (Figure 1C and 1D), demonstrating that it does not inhibit HER2 phosphorylation. Furthermore, consistent with our data (Figure 1E), mubritinib has been reported to display no activity against almost 300 other kinases screened [24].

Because mubritinib affects signalling pathways associated with a decrease in cellular energy, and because inhibiting mitochondrial respiration could have particularly deleterious effects on tissues with high energy demand such as the heart, we tested the effect of mubritinib on ATP production in H9c2 cardiomyoblasts [25] and human embryonic stem cell derived cardiomyocytes (hESC-CM, GE Healthcare) using the glucose/galactose system. In galactose-containing media cells are predominantly reliant on mitochondria for the production of cellular ATP, allowing mitochondrial liabilities that are masked in glucose to be revealed [26,27].

Exposure of H9c2 cells to 2 μM mubritinib for 2 hours in galactose-containing media led to a 50% decrease in ATP levels (Figure 1F). Furthermore, prolonged exposure depleted ATP levels to 10% of the control value (Figure 1F) and induced cell death (Figure 1G). Importantly, inhibition of ATP production in galactose (but not glucose) containing media by mubritinib and other inhibitors of oxidative phosphorylation was also observed in hESC-CMs (Figure 1H) and had a profound effect on cell beat rate (Figure 1I).

Structure activity relationships (SARs) determined using a library of derivatives to identify a novel toxicophore in mubritinib

It has been shown recently that mubritinib targets respiratory complex I and inhibits growth of cancer cells from patients with AML, which are highly dependent on oxidative phosphorylation for survival [16]. Therefore, to understand likely toxicities associated with such treatments, we investigated whether complex I is similarly affected in cardiomyocytes exposed to mubritinib (**1**), and used a focussed chemical library of mubritinib derivatives (**2**-**8**) to identify the potential toxicophore (Figure 2A). The mubritinib variants were synthesised with modifications in two regions of the molecule; the aryl trifluoromethyl group (compounds **2**-**4**) and the triazole group (compounds **5**-**8**).

The oxygen consumption rates (OCR) of H9c2 and hESC-CM cells treated with mubritinib (**1**) were measured to determine whether the decreased ATP content in galactose containing media (Figures 1F and 1H) were due to direct inhibition and/or uncoupling of the respiratory chain [28]. As expected, oligomycin A, which inhibits ATP synthase, had no effect on the rotenone-sensitive OCR in the presence of the uncoupling agent FCCP (carbonyl cyanide-4-(trifluoromethoxy) phenylhydrazone). However, in H9c2 or hESC-CMs cells exposed to mubritinib the rotenone-sensitive OCR decreased by ~50% (Figure 2B and Figure 2- figure supplement 1 A and B). Taken together, these data suggest that mubritinib (**1**) inhibits the mitochondrial respiratory electron transport chain in cardiomyocytes.

The effects of mubritinib (**1**) on complex I and II linked respiration were then determined in plasma-membrane permeabilised H9C2 cells. First, cells were pre-treated with increasing doses of mubritinib (**1**), or the complex I inhibitor rotenone or the complex III inhibitor

antimycin A. As expected, all inhibitor treatments decreased the OCR (Figure 2C). Cells were then treated with plasma membrane permeabiliser followed by addition of ADP. Pyruvate/malate and succinate were used to drive respiration from complex I and complex II, respectively and, in untreated cells, they both stimulated the OCR. All three inhibitors inhibited pyruvate/malate-driven respiration but, crucially, the inhibition of only mubritinib and rotenone was alleviated by subsequent treatment with succinate (Figure 2C), suggesting that mubritinib is a complex I inhibitor.

Mitochondrial membranes were then used to assess the effect of mubritinib (**1**) on complex I and complex II driven respiration directly. In agreement with the data obtained from cell lines, mubritinib (**1**) showed a dose-dependent decrease in the rate of NADH oxidation and no effect on succinate oxidation (Figures 2D and 2E). The NADH oxidation data were then fit to the standard dose-effect relationship and yielded an IC_{50} value of 19.2 nM (Figure 2D).

Purified complex I was then used to confirm inhibition of complex I unambiguously, and to dissect whether mubritinib (**1**) inhibits it at its NADH or ubiquinone binding site. NADH oxidation was coupled to reduction of either the ubiquinone-10 analogue decyclubiquinone (dQ) or to reduction of an artificial electron acceptor ($APAD^+$ or ferricyanide, FeCN) that reoxidises the flavin in the NADH binding site directly [29 30], without the involvement of ubiquinone (Figure 2E) [29]. While $APAD^+$ and FeCN reduction were unaffected at 500 nM mubritinib (**1**), the rate of ubiquinone reduction was essentially abolished (Figure 2E). These data confirm that mubritinib inhibits complex I directly by inhibiting ubiquinone reduction, most likely by binding in the ubiquinone-binding site.

The variants of mubritinib were then tested for their ability to inhibit complex I in mitochondrial membranes (Figure 2F and Figure 2-figure supplement 2 Ai-viii). Compounds **2-4** (Figure 2A), which have the same N^1-linked triazole moiety as mubritinib but contain either no substituent (**2**) or a mild (**3**) or strong (**4**) electron donating group in the para-position of the phenyl ring, retain the ability to inhibit complex I, similarly to mubritinib (Figure 2F). In contrast, compound **6**, which has the 1,2,3-triazol-1-yl moiety substituted for an isomeric 1,2,3-triazol-2-yl group, is a much weaker inhibitor (Figure 2F). Complete removal of the triazole group in **5** and modification of the triazole to an *N*-linked pyrrole in **8**, also resulted in compounds that no longer inhibited NADH oxidation (Figure 2F). Most interestingly, modification of the triazole to the *N*-linked imidazole **7** retained the inhibitory activity. These data provide strong evidence that a 1,3-amidine-like motif, housed within the 1*H*-1,2,3-triazol-1-yl substituent, is required for complex I inhibition. The same pattern of inhibition was observed for ATP production in cells grown in media containing galactose (Figure 2G). Therefore, inhibition of ATP production by mubritinib results from the inhibition of complex I, and depends strongly upon its 1,2,3-triazol-1-yl moiety and the embedded toxicophore.

The 1,2,3-triazol-1-yl toxicophore in carboxyamidotriazole (CAI) inhibits ATP production, mitochondrial function and cell proliferation

Based on the 1*H*-1,2,3-triazol-1-yl moiety being critical for the function of mubritinib we initially searched for other compounds that contain a 1,2,3-triazol-1-yl or similar moiety that might display analogous toxicity profiles. A structural similarity search carried out on the ChEMBL database revealed a range of terminal 1,2,3-triazole-containing drugs as putative complex I inhibitors (Supplementary File 1) including carboxyamidotriazole (**9**, Figure 3A),

215 which has been trialled widely as an anticancer agent in single and combination therapies to
216 treat glioblastoma, ovarian cancer and non-small cell lung cancer [19, 20]. Data from a number
217 of studies have suggested that the anti-proliferative and anti-metastatic properties of CAI (**9**)
218 are mediated through the inhibition of non-voltage gated Ca^{2+} channels in non-excitable cells
219 [31], which in turn modulates downstream phosphorylation events [32], however this has not been
220 demonstrated directly. Calcium binding assays performed here show clearly that there is no
221 significant binding of CAI (**9**) to non-voltage gated Ca^{2+} channels (Supplementary File 2). It
222 has also been shown that CAI (**9**) affects mitochondrial calcium import and local calcium
223 clearance, which is essential for the maintenance of capacitative calcium entry [33] and it was
224 proposed that this then inhibited oxidative phosphorylation [34]. These data suggest that the
225 toxicophore, in the context of CAI (**9**), might act in a similar way to mubritinib, and that the
226 effects on mitochondrial calcium release could be the secondary effects of complex I
227 inhibition. To explore the effect of the heterocycle in CAI (**9**) on mitochondrial function we
228 generated three variants. Two compounds, which we predicted by analogy with our
229 mubritinib variants that would be inactive, contained isomeric pyrazoles (**10** and **11**). One
230 further compound was synthesised where the triazole ring in CAI was replaced with an
231 imidazole ring (**12**), which we predicted would retain mitochondrial toxicity (Figure 3A).
232 The set of compounds was then tested in H9c2 cardiomyoblasts for their effects on oxygen
233 consumption rates and ATP production (Figure 3B and 3C). CAI (**9**) and compound **12**
234 inhibited ATP production in galactose containing media much more strongly than compounds
235 **10** and **11** (Figure 3B). Similarly, CAI (**9**) and compound **12** decreased oxygen consumption
236 rates much more effectively than compounds **10** and **11** (Figure 3C and Figure 3-figure
237 supplement 1).
238

Given that CAI has been trialled as an anti-cancer therapeutic against lung cancer [20], CAI (**9**) and compounds **10** and **11** were tested in the lung cancer derived cell line, A459, to determine whether the effects on mitochondrial function observed in the Hc92C cardiomyoblasts were replicated. The data show that CAI (**9**) inhibits ATP production in A549 cells grown in galactose, whereas **10** and **11** have minimal effect (Figure 3D) with no difference observed, as expected, in glucose containing media (Figure 3-figure supplement 1C). Moreover, the basal and maximal OCR of cells treated with CAI (**9**) were significantly reduced, with a much smaller decrease observed with compounds **10** and **11** (Figure 3E and Figure 3-figure supplement 1).

To confirm that CAI inhibited complex I, A549 cells were treated with PMP followed by addition of ADP, pyruvate and malate (Figure 3F). In untreated cells, or cells treated with **10** and **11**, there was a large increase in oxygen consumption as expected, however, oxygen consumption was inhibited in cells treated with CAI (**9**), antimycin A or piericidin. Following addition of succinate and ADP there was an increase OCR in CAI (**9**) and piericidin-treated cells (but not in cells treated with antimycin A), strongly suggesting that CAI (**9**) is a complex I inhibitor. Importantly, given that compounds **10** and **11** only have a small effect, in this chemical context the triazolyl toxicophore contributes in a similar manner to mubritinib.

To confirm these data, mitochondrial membranes were used to assess the impact of each compound on complex I-driven respiration. As expected, both CAI (**9**) and **12** inhibited complex I-driven respiration whereas compounds **10** and **11** have essentially no effect (Figure 3G), as reflected by the measured IC_{50} values for each compound (Figure 3-figure supplement 2). Similar to mubritinib, inhibition of complex I with CAI also effects signalling pathways downstream of the energy sensor AMPK, such as increased ACC phosphorylation and inhibition of mTOR signalling reducing RPS6 phosphorylation (Figure 3-figure

supplement 3). Importantly these pathways are unaffected by the non-specific calcium channel inhibitor bebridil hydrochloride or the inactive CAI variant compound **11**.

Inhibition of cell proliferation and cell death by CAI and mubritinib via complex I inhibition is dependent on the toxicophore

To confirm that the toxicophore we have identified is directly linked to the reported anti-proliferative/cancer chemotherapeutic properties of mubritinib (**1**) and CAI (**9**), the degree of cell death following treatment with these compounds was measured in a range of cancer derived cell lines. The cells lines used were representative of AML (HL60), glioblastoma (M059K), lung (A549), osteosarcoma (U-20S), in addition to HeLa cells since these cancers display varying degrees of dependence on glycolysis versus oxidative phosphorylation for energy production and to provide key metabolites required for tumour cell survival [35, 36]. Cells were grown in galactose or glucose containing media in the presence of mubritinib (**1**), CAI (**9**), or a corresponding inactive variant, **5** or **11** respectively, and the degree of cell death was measured using DRAQ7™ staining and Annexin-V-FITC labelling (Figure 4 and Figure 4-figure supplement 1). The data show that treatment of the AML derived cell line with either CAI (**9**) or mubritinib (**1**) caused cell death in both glucose and galactose, while the analogue compounds which lacked the heterocyclic 1,3-nitrogen motif had no effect (Figure 4A and 4B, Figure 4-figure supplement 1). The other cell lines used showed no cell death in the presence of glucose (Figure 4D, 4F and Figure 4-figure supplement 1D, F and G), however again there was a correlation between the presence of the toxicophore and cell death in galactose (Figure 4C, 4E and Figure 4-figure supplement 1C, E and H). To explore whether the toxicophore had similar effects on cell growth, BT474 (Figure 4G) and A549 (Figure 4H) cells were grown in glucose and proliferation measured using xCELLigence

RTCA DP instrument. Again, the data show a direct correlation between the presence of the 1,2,3-triazole and cell growth inhibition as both mubritinib (**1**) and CAI (**9**) slowed cell growth, whereas the analogues, which lacked the heterocyclic 1,3-nitrogen motif, had reduced or no effect.

Taken together these data establish that the presence of the triazole and its embedded heterocyclic 1,3-nitrogen toxicophore is essential for the parent drug effects on tumour cell growth of otherwise chemically distinct mubritinib and CAI.

Discussion

Our data show the value of using SARs to probe the molecular signatures that potentially trigger toxicity pathways and, through the identification of a novel toxicophore, have implications for drug development programmes (Figure 5). The toxicophore in the context of mubritinib and CAI is the embedded 1,3-nitrogen motif of the 1*H*-1,2,3-triazol-1-yl heterocycle and we have shown that this nitrogen atom disposition appears critical for both mitochondrial toxicities (Figures 1-4). In a preliminary screen of compounds that inhibited complex I, we identified two antifungal agents, ketoconazole and terconazole, which also contained the heterocyclic 1,3-nitrogen motif embedded within a 1*H*-1,2,4-triazol-1-yl or 1*H*-imidazol-1-yl substituent respectively (Supplementary File 3). Interestingly, we also found that rufinamide (Supplementary File 1), which contains a chemically similar core scaffold to CAI, displayed no complex I inhibitory activity [37]. However, there are key structural differences between these two drugs and in particular, rufinamide lacks an anilino nitrogen in the 5-position of the 1,2,3-triazole, the *para*-chlorobenzoyl moiety and there is a chloro to fluoro switch with regards the halogen substituents on the *N*-benzyl group (alongside the switch in position from 3,5 to 2,6). These observations are therefore coupled with a

difference in the logP of rufinamide (1.3) when compared to CAI (3.1) which indicates a significant decrease in its overall lipophilicity and may therefore reflect a compromised pharmacokinetic-driven target engagement . Which of these differences drive the observed loss in complex I inhibition by rufinamide is a focus of ongoing work.

It is of serious concern that while both mubritinib and CAI are trialled as part of anti-cancer therapies[16], neither directly bind their reported targets, HER2 and Ca^{2+} channels respectively (Figure 1 and Supplementary File 2). Mitochondria play a central role in cell-wide processes in addition to bioenergetics and metabolism by providing a signalling hub that controls stemness, differentiation and apoptosis [13], therefore disruption of mitochondrial function can easily be misattributed to other targets, such as receptors involved in cell signalling. Cardiac cells are especially sensitive to mitochondrial toxicants that alter ATP production and our data suggest that both mubritinib and CAI have the potential to affect these cell types in situations when glucose is limiting (Figures 1, 2 and 4). It would therefore be important to monitor patients treated with such agents for changes in cardiac function during future clinical trials of CAI or mubritinib.

In terms of cancer treatment, mubritinib has been used to chemo-sensitise tumour cells to other cytotoxic agents. For example, in combination with AC220 (quizartinb), mubritinib reduces the viability of ovarian derived cell lines [15]. However, sole inhibition of complex I is also a viable treatment option for some cancer types. Thus while drugs that target the coordinated upregulation of glycolysis that is often associated with tumorigenesis are being developed, several studies have shown that many cancer cell subpopulations are particularly dependent upon OXPHOS for bioenergetic and biosynthetic processes [38-40]. Compounds that target the mitochondria, either complex I including mubritinib [16] and IACS-010759[35], or the ATP synthase such as Giboxin [36], have been shown to have efficacy in glycolysis–deficient tumour cells derived from patients with AML and glioblastoma[16, 32, 36]. Interestingly, IACS-

010759[32] contains a 1*H*-1,2,4-triazole suggesting a similar mode of action of this drug since this heterocycle also possesses the amidine-like nitrogen substitution pattern.

Since the efficacy of both mubritinib and CAI (Figure 4) is dependent upon an amidine-like nitrogen substructure our data suggest that new drug development programmes using this substructure within the correct chemical context could be employed to devise therapies for glycolysis deficient tumours, providing that cardiac liabilities are assessed and evaluated. Therefore, a more detailed examination of potential molecular recognition of these and other substructures by complex I is ongoing within our laboratories, coupled with consideration of target access from a pharmacokinetic perspective to allow repurposing of a number of drugs for their anti-cancer properties.

Material and Methods

Cell Culture

All cell lines were obtained from ATCC, except hESC-cardiomyocytes which were obtained from GE healthcare (Cytiva™ Plus, GE Healthcare). Glucose containing media consists of glucose-containing DMEM (Life Technologies, Gibco® 41966) supplemented with 10% FBS. Galactose containing media consists of glucose-free DMEM (Life Technologies, Gibco®) supplemented with 10 mM galactose, 200 mM L-glutamine, 100 mM sodium pyruvate and 10% FBS. Prior to treatments, cells were grown in their respective media overnight. hESC-cardiomyocytes were cultured in RPMI-1640 media supplemented with either glucose (11 mM) or galactose (10 mM). All cell lines were routinely tested to ensure that they were mycoplasma free.

Western blot analyses

Whole cell lysates were prepared in lysis buffer (50 mM Tris pH 7.5, 150 mM sodium chloride, 1% Triton X-100, 0.1% SDS, 0.5% sodium deoxycholate, 1X Roche protease inhibitor cocktail and 1X Roche PhosStop phosphatase inhibitor cocktail). Protein amount was quantified using Pierce BCA protein assay kit (ThermoFisher scientific) and 25 μg protein was separated using SDS-PAGE and transfered to PVDF membranes. Primary antibodies used: phospho-HER2 (Y1221/1222) (CST, #2243), HER2 (CST, #2165), phospho-ACC (S-79) (CST, #3661), ACC (CST, #3676), phospho-RPS6 (S240/244) (CST, #2215), RPS6 (CST, #2217), β-tubulin (CST, #2146). Secondary antibodies used: IR-dye labelled α-rabbit (CST, #5366S). Fluorescent signal was detected using LI-COR Odyssey imaging system (LI-COR biosciences) and images analysed with LI-COR image studio software (package version 5.2.5).

Measurement of ATP content

H9c2 rat cardiomyoblast cells and hESC-cardiomyocytes were seeded in 96 well plates at a density of 7 x 10^3 and 3.6 x 10^5 cells per well respectively, whereas A549 cells were seeded at a density of 1 x 10^4 cells per well. ATP concentrations were measured using the Promega Cell Titer Glo assay according to manufacturer's protocol.

Measurement of bioenergetics in live cells

An Agilent XF Seahorse Analyzer was used to measure respiration and glycolysis in intact cells in real time. Cells were seeded in Seahorse Biosciences XF24 plates. H9c2, hESC-CM (Cytiva^{TM} Plus, GE Healthcare) and were seeded at 9 x 10^4, and 6 x 10^4 cells per well (coated with 25 µl fibronectin prior to seeding). Prior to the assay, media was replaced with DMEM, containing either glucose or galactose. Drugs were dissolved in DMSO and injected from pre-loaded ports pneumatically.

Measurement of mitochondrial respiration in permeabilised cells

Cholesterol-dependent permeabilser XF Plasma Membrane Permeabiliser (PMP) (Seahorse Biosciences), was used as described[41]. Mitochondrial assay buffer or mannitol and sucrose buffer (MAS, pH 7.2) (220 mM mannitol, 70 mM sucrose, 10 mM KH_2PO_4, 5 mM $MgCl_2$, 2 mM HEPES, 1 mM EGTA, 4 mg/ml BSA, was used. Cells were seeded at 5 x 10^4 per well in XF Cell Culture plates in standard culture medium. Cells were washed once with MAS before addition of pre-warmed MAS at a final volume of 675 µl. Pyruvate (5 mM), malate (2.5 mM) and ADP (1 mM) were added for measurement of complex I-driven respiration and succinate (10 mM) and ADP (1 mM) for complex II-driven respiration.

Preparation of proteins and mitochondrial membranes

401 Mitochondrial membranes and complex I were prepared from bovine (*Bos taurus*) heart
402 mitochondria as described previously [42,43].
403
404 ***NADH oxidation assays by mitochondrial membranes and complex I***
405 Assays were performed in 10 mM Tris SO_4 (pH 7.5), 250 mM sucrose at 32 °C. For
406 measurement of NADH:O_2 oxidoreduction, 20-30 μg mL^{-1} of membranes, 1 or 3 μM horse
407 heart cytochrome *c*, and 120 or 200 μM NADH were added and the absorbance of NADH
408 measured at 340-380 nm using linear regression, once steady-state was reached. Succinate
409 oxidation was determined using a coupled enzymatic assay [44] in the presence of 5 mM
410 succinate. NADH:decylubiquinone (dQ), NADH: 3-acetylpyridine adenine dinucleotide
411 ($APAD^+$), and NADH:ferricyanide (FeCN) oxidoreduction by complex I were measured
412 using 0.5 μg mL^{-1} complex I, 100 μM NADH, 0.075% soy bean asolectin (Avanti Polar
413 Lipids), 0.075% 3-[(3-Cholamidopropyl)dimethylammonio]-1-propanesulfonate (CHAPS,
414 Merck Chemicals Ltd,) and 100 μM dQ, 500 μM $APAD^+$ or 1 mM FeCN, respectively.
415
416 ***Quantification of cardiac cell function in hESC-CM using multi-electrode arrays (MEA)***
417 MEA plates (Axion Biosystems, M768-KAP-48) contain 48 wells, each with 16 electrodes.
418 hESC-CM were grown on these plates and incubated with the doses of mubritinib shown and
419 recordings were taken over a time course up to 72 hours. AxIS (Version 2.0.2.9) cardiac beat
420 detector which uses an inflection search algorithm was used to detect changes in cardiac
421 action potential.

Apoptosis and cell death analysis

For analysis of cell death and apoptosis, cells were harvested and FITC-conjugated Annexin-V antibody and far-red DNA stain DRAQ7™ were added to pellets resuspended in Annexin-V Binding Buffer (BD Pharmingen). Samples were analysed by flow cytometry using the FITC and APC channels.

Assays for ion channel binding

Ion channel binding assays were carried out by Eurofins Panlabs Discovery Services Taiwan Ltd. The binding affinity of compounds to ion channels was measured using an in vitro radioligand binding assay ([^{3}H] 1,4,5-IP3) in rat cerebellum, following incubation at 25 ^{o}C for 10 minutes. All data are displayed show a percentage binding of each compound relative to control 1,4,5-IP3.

Assays for activity against HER2

A radiometric kinase assay was carried out by Eurofins Ltd. In brief, the effect of mubritinib on recombinant human HER2 activity was determined by measuring the incorporation of radioactive ^{32}P-ATP using concentrations from 10 nM to 10 μM. Activity values represent the percentage relative to the positive control. Mubritinib was also tested for activity against EGFR, ErbB4, Flt1 and PDGRα at a concentration of 1 μM. Lapatinib was tested against HER2 as a positive control. The experiments were carried out in triplicate and the counts per minute (CPMs) were normalised to the control.

Cell proliferation assays

Cell proliferation assays were performed in a standard CO_2 incubator using the xCELLigence RTCA DP instrument (ACEA Biosciences) according to manufacturer's instructions. Microelectrode sensor arrays embedded on the base of the E-plate 16 (ACEA Biosciences) measure changes in impedance as cells attach and proliferate, enabling label free quantification of cell proliferation. A549 or BT474 cells were seeded on an E-plate 16 in a total volume of 150 µl media. Cells were allowed to attach to the plate and enter log phase growth (~ 20 hours) before treatment with indicated compounds of interest. Cell proliferation was monitored for 96 hours post treatment and all treatments were performed in at least technical duplicate and biological triplicate.

Chemical Synthesis

For synthesis of mubritinib and CAI variants see supplementary material.

Additional information

The authors declare no conflicts of interest

Acknowledgements

This work was funded by the Medical Research Council (MC_UU_000 /RG94521 and PUAG015 to AEW and MC_U105663141 and MC_UU_00015/2 to JH) and by an ITTP studentship to ZAS. Thanks to Ryan Mordue for drawing Figure 5.

References

1. Morgan, P. *et al.* Impact of a five-dimensional framework on R&D productivity at AstraZeneca. *Nature reviews. Drug discovery* **17**, 167-181 (2018).
2. Dey, S., Luo, H., Fokoue, A., Hu, J. & Zhang, P. Predicting adverse drug reactions through interpretable deep learning framework. *BMC bioinformatics* **19**, 476 (2018).
3. Allen, T.E.H., Goodman, J.M., Gutsell, S. & Russell, P.J. Using 2D Structural Alerts to Define Chemical Categories for Molecular Initiating Events. *Toxicological sciences:* **165**, 213-223 (2018).

4. Uetrecht, J. & Naisbitt, D.J. Idiosyncratic adverse drug reactions: current concepts. *Pharmacological rev* **65**, 779-808 (2013).
5. Will, Y. & Dykens, J. Mitochondrial toxicity assessment in industry--a decade of technology development and insight. *Expert opinion on drug metabolism & toxicology* **10**, 1061-1067 (2014).
6. Dykens, J.A. & Will, Y. The significance of mitochondrial toxicity testing in drug development. *Drug discovery today* **12**, 777-785 (2007).
7. Johnson, D.T., Harris, R.A., Blair, P.V. & Balaban, R.S. Functional consequences of mitochondrial proteome heterogeneity. *American journal of physiology. Cell physiology* **292**, C698-707 (2007).
8. Johnson, D.T. *et al.* Tissue heterogeneity of the mammalian mitochondrial proteome. *American journal of physiology. Cell physiology* **292**, C689-697 (2007).
9. Calvo, S.E. & Mootha, V.K. The mitochondrial proteome and human disease. *Annual rev of genomics and human genetics* **11**, 25-44 (2010).
10. El-Hattab, A.W. & Scaglia, F. Mitochondrial Cardiomyopathies. *Frontiers in cardiovascular medicine* **3**, 25 (2016).
11. Kolwicz, S.C., Jr., Purohit, S. & Tian, R. Cardiac metabolism and its interactions with contraction, growth, and survival of cardiomyocytes. *Circulation research* **113**, 603-616 (2013).
12. Meyer, J.N., Hartman, J.H. & Mello, D.F. Mitochondrial Toxicity. *Toxicological sciences :* **162**, 15-23 (2018).
13. Guerra, F. *et al.* Mitochondrial Dysfunction: A Novel Potential Driver of Epithelial-to-Mesenchymal Transition in Cancer. *Frontiers in oncology* **7**, 295 (2017).
14. Nagasawa, J. *et al.* Novel HER2 selective tyrosine kinase inhibitor, TAK-165, inhibits bladder, kidney and androgen-independent prostate cancer in vitro and in vivo. *International journal of urology : o* **13**, 587-592 (2006).
15. Ouchida, A.T. *et al.* Synergistic effect of a novel autophagy inhibitor and Quizartinib enhances cancer cell death. *Cell death dis* **9**, 138 (2018).
16. Baccelli, I. *et al.* Mubritinib Targets the Electron Transport Chain Complex I and Reveals the Landscape of OXPHOS Dependency in Acute Myeloid Leukemia. *Cancer cell* **36**, 84-99.e88 (2019).
17. Sridhar, S.S., Seymour, L. & Shepherd, F.A. Inhibitors of epidermal-growth-factor receptors: a review of clinical research with a focus on non-small-cell lung cancer. *The Lancet. Oncology* **4**, 397-406 (2003).
18. Omuro, A. *et al.* Multicenter Phase IB Trial of Carboxyamidotriazole Orotate and Temozolomide for Recurrent and Newly Diagnosed Glioblastoma and Other Anaplastic Gliomas. *Journal of clinical oncology :* **36**, 1702-1709 (2018).
19. Azad, N. *et al.* A phase I study of paclitaxel and continuous daily CAI in patients with refractory solid tumors. *Cancer biology & therapy* **8**, 1800-1805 (2009).
20. Johnson, E.A. *et al.* Phase III randomized, double-blind study of maintenance CAI or placebo in patients with advanced non-small cell lung cancer (NSCLC) after completion of initial therapy (NCCTG 97-24-51). *Lung cang* **60**, 200-207 (2008).
21. Brandao, M. *et al.* Combination therapies for the treatment of HER2-positive breast cancer: current and future prospects. *Expert review of anticancer therapy* **18**, 629-649 (2018).
22. Sica, V., Bravo-San Pedro, J.M., Stoll, G. & Kroemer, G. Oxidative phosphorylation as a potential therapeutic target for cancer therapy. *International journal of cancer* (2019).
23. Leibovitch, M. & Topisirovic, I. Dysregulation of mRNA translation and energy metabolism in cancer. *Advances in biological regulation* **67**, 30-39 (2018).

24. Anastassiadis, T., Deacon, S.W., Devarajan, K., Ma, H. & Peterson, J.R. Comprehensive assay of kinase catalytic activity reveals features of kinase inhibitor selectivity. *Nature biotechnology* **29**, 1039-1045 (2011).
25. Kimes, B.W. & Brandt, B.L. Properties of a clonal muscle cell line from rat heart. *Experimental cell research* **98**, 367-381 (1976).
26. Marroquin, L.D., Hynes, J., Dykens, J.A., Jamieson, J.D. & Will, Y. Circumventing the Crabtree effect: replacing media glucose with galactose increases susceptibility of HepG2 cells to mitochondrial toxicants. *Toxicological sciences :* **97**, 539-547 (2007).
27. Rana, P., Nadanaciva, S. & Will, Y. Mitochondrial membrane potential measurement of H9c2 cells grown in high-glucose and galactose-containing media does not provide additional predictivity towards mitochondrial assessment. *Toxicology in vitro :* **25**, 580-587 (2011).
28. Felser, A., Blum, K., Lindinger, P.W., Bouitbir, J. & Krahenbuhl, S. Mechanisms of hepatocellular toxicity associated with dronedarone--a comparison to amiodarone. *Toxicological sciences :* **131**, 480-490 (2013).
29. Birrell, J.A., Yakovlev, G. & Hirst, J. Reactions of the flavin mononucleotide in complex I: a combined mechanism describes NADH oxidation coupled to the reduction of APAD+, ferricyanide, or molecular oxygen. *Biochemistry* **48**, 12005-12013 (2009).
30. Yakovlev, G. & Hirst, J. Transhydrogenation reactions catalyzed by mitochondrial NADH-ubiquinone oxidoreductase (Complex I). *Biochemistry* **46**, 14250-14258 (2007).
31. Hupe, D.J., Behrens, N.D. & Boltz, R. Anti-proliferative activity of L-651,582 correlates with calcium-mediated regulation of nucleotide metabolism at phosphoribosyl pyrophosphate synthetase. *Journal of cellular physiology* **144**, 457-466 (1990).
32. Bauer, K.S., Cude, K.J., Dixon, S.C., Kruger, E.A. & Figg, W.D. Carboxyamido-triazole inhibits angiogenesis by blocking the calcium-mediated nitric-oxide synthase-vascular endothelial growth factor pathway. *The Journal of pharmacology and experimental therapeutics* **292**, 31-37 (2000).
33. Mignen, O. *et al.* Carboxyamidotriazole-induced inhibition of mitochondrial calcium import blocks capacitative calcium entry and cell proliferation in HEK-293 cells. *Journal of cell science* **118**, 5615-5623 (2005).
34. Ju, R. *et al.* Carboxyamidotriazole inhibits oxidative phosphorylation in cancer cells and exerts synergistic anti-cancer effect with glycolysis inhibition. *Cancer letters* **370**, 232-241 (2016).
35. Molina, J.R. *et al.* An inhibitor of oxidative phosphorylation exploits cancer vulnerability. *Nature medicine* **24**, 1036-1046 (2018).
36. Shi, Y. *et al.* Gboxin is an oxidative phosphorylation inhibitor that targets glioblastoma. *Nature* **567**, 341-346 (2019).
37. Serreli, R. Pharmacological aspects of the inhibition of mammalian respiratory complex I *University of Cambridge Doctoral thesis* (2018).
38. Vazquez, F. *et al.* PGC1alpha expression defines a subset of human melanoma tumors with increased mitochondrial capacity and resistance to oxidative stress. *Cancer Cell* **23**, 287-301 (2013).
39. Viale, A. *et al.* Oncogene ablation-resistant pancreatic cancer cells depend on mitochondrial function. *Nature* **514**, 628-632 (2014).
40. Birsoy, K. *et al.* An Essential Role of the Mitochondrial Electron Transport Chain in Cell Proliferation Is to Enable Aspartate Synthesis. *Cell* **162**, 540-551 (2015).

41. Salabei, J.K., Gibb, A.A. & Hill, B.G. Comprehensive measurement of respiratory activity in permeabilized cells using extracellular flux analysis. *Nature protocols* **9**, 421-438 (2014).
42. Blaza, J.N., Serreli, R., Jones, A.J., Mohammed, K. & Hirst, J. Kinetic evidence against partitioning of the ubiquinone pool and the catalytic relevance of respiratory-chain supercomplexes. *Proceedings of the National Academy of Sciences of the United States of America* **111**, 15735-15740 (2014).
43. Jones, A.J. *et al.* A Self-Assembled Respiratory Chain that Catalyzes NADH Oxidation by Ubiquinone-10 Cycling between Complex I and the Alternative Oxidase. *Angewandte Chemie* **55**, 728-731 (2016).
44. Jones, A.J. & Hirst, J. A spectrophotometric coupled enzyme assay to measure the activity of succinate dehydrogenase. *Analytical Biochemistry* **442**, 19-23 (2013).
43. Jhaveri, Z.,Woo, J., Shang X., Park BH., Gabrielson, E. AMP-activated kinase (AMPK) regulates activity of HER2 and EGFR in breast cancer *Oncotarget* **6**:14754-14765 (2015)

Figure 1: Mubritinib does not inhibit HER2, but inhibits ATP production and beat rate of cardiomyocytes

A) Western blot analysis of the HER2-overexpressing cell line, BT474, treated with increasing doses of mubritinib. HER2 activity was assessed with antibodies against phosphorylated HER2 (Y1221/1222). Cells were treated with the clinically used HER2 inhibitor, lapatinib (10 μM), as a positive control.

B) Western blot analysis of the HER2-overexpressing cell line, BT474, treated with 1 μM of either mubritinib, lapatinib, compound 5 (inactive mubritinib derivative, see Figure 2A), antimycin A or rotenone for 2 hours.

C) Radiometric kinase assays were carried out and the effect of mubritinib (at the concentrations shown) on recombinant human HER2 activity was determined by measuring the incorporation of radioactive 32P-ATP after 15 mins. Activity values are displayed relative to the untreated sample.

D) Radiometric kinase assays were carried out using recombinant human HER2 in the presence of 1 μM mubritinib and lapatinib (DMSO control and lapatinib, n = 3, mubritinib, n = 2). Significance following lapatinib treatment was assessed using the unpaired students t-test (*** $p < 0.001$) relative to the DMSO control.

E) Radiometric kinase assays were carried out on recombinant human EGFR, ErbB4, Flt1 and PDFRa in the presence of 2 μM mubritinib. Error bars represent standard deviation (n = 3).

F) A 24 hour time course for loss of ATP from H9c2 cells following treatment with 2 μM mubritinib in media containing either glucose or galactose as the carbon source. Error bars represent standard deviation (n = 3) and significance was assessed using ANOVA with Dunnett's multiple comparisons test (**** $p < 0.0001$, *** $p < 0.001$, ns = not significant).

G) H9c2 cells were treated with 2 μM mubritinib in media containing either glucose or galactose as the carbon source and cell viability was assessed over a 72-hour period using DRAQ7™ staining and Annexin-V-FITC labelling. Error bars represent standard deviation (n = 3) and significance at each time point was assessed using ANOVA with Tukey's multiple comparisons test (**** $p < 0.0001$).

H) hESC-cardiomyocytes (CytivaTM Plus, GE Healthcare) were grown in RPMI-1640 media supplemented with galactose (10 mM) or glucose (11 mM) and treated with 1 μM of mubritinib, or inhibitors of mitochondrial complex III (antimycin A), ATP synthase (oligomycin A) or complex I (rotenone). ATP levels were measured after 2 hours. Error bars

represent standard deviation (n = 4) and significance was assessed using the unpaired students t-test (**** $p < 0.0001$).

I) hESC-cardiomyocytes (CytivaTM Plus, GE Healthcare) were grown in either galactose (10 mM) or glucose (11 mM) containing media on multi-electrode array plates from which it is possible to assess beat rate. The average beat rates in glucose (i) and galactose (ii) containing media of 52.2 and 30.7 BPM respectively, were set to 100%. Cells were treated with mubritinib (1 μM), antimycin A (1 μM) or rotenone (1 μM). Error bars represent standard deviation (n = 3) and significance was assessed using the unpaired students t-test (* $p < 0.05$, ** $p < 0.01$, **** $p < 0.0001$).

Figure 2: Mubritinib is an inhibitor of mitochondrial complex I

A) Variants of mubritinib were synthesised with alterations to the trifluoromethylphenyl group (2, 3 and 4) or the triazole (5, 6, 7 and 8). Mubritinib (1) and mubritinib synthesised "in house" were used as positive controls.

B) Rotenone-sensitive oxygen consumption rates (OCRs) of H9c2 or hESC-CM cells in glucose containing media were measured after the addition of FCCP in the presence of either 1 μM mubritinib or 1 μM oligomycin A. OCR values are represented relative to untreated cells and error bars represent standard deviation (n = 3). Significance was assessed using the unpaired students t-test (*** $p = < 0.001$, **** $p = < 0.0001$, ns = not significant).

C) OCR was measured in cells pre-treated with 0.5 μM, 2 μM and 10 μM mubritinib, 1 μM rotenone or 10 μM antimycin A using a Seahorse XF Analyzer. PMP was added to permeabilise the plasma membrane, followed by pyruvate, malate and ADP to drive complex I linked respiration. Then, rotenone was added to abolish complex I respiration followed by ADP and succinate to drive complex II linked respiration. Error bars represent standard deviation (n = 3).

D) Mubritinib was incubated with mitochondrial membranes from bovine heart at the concentrations shown, then the rate of NADH was measured spectrophotometrically. Error bars represent standard error of the mean (n = 3). Data were fit using activity (%) = 100 / (1 + (IC_{50} / [inhibitor]) Hill slope and yielded an IC_{50} value of 19.2 nM.

E) Relative rates of NADH or succinate oxidation by mitochondrial membranes or complex I isolated from bovine heart using O_2, dQ, APAD+, or FeCN as the electron acceptor in the presence of 500 nM mubritinib. Error bars represent standard deviation (n = 3) and significance was assessed using ANOVA with Dunnett's multiple comparisons test (**** $p <$ 0.0001, ns = not significant).

F) Mubritinib and the variants from (A) were incubated with mitochondrial membranes at 500 nM. The rate of NADH oxidation was measured spectrophotometrically. The activity is expressed relative to the DMSO control, set to 100%. Error bars represent standard deviation (n = 3) and significance was assessed using ANOVA with Dunnett's multiple comparisons test (**** $p < 0.0001$, ** $p < 0.01$). Activities were inter/extrapolated from measured data points for compounds 7 and 8.

G) H9c2 cells were treated with mubritinib and all compound variants (10 μM) in galactose containing media for 24 hours and ATP levels were measured. Error bars represent standard deviation (n = 3) and significance was assessed using ANOVA with Dunnett's multiple comparisons test (**** $p < 0.0001$, ns = not significant).

Figure 3: The toxicophore present in carboxyamidotriazole inhibits mitochondrial complex I

A) Chemical structure of carboxyamidotriazole (CAI) (9) and three variants whereby the core triazole ring was replaced with either a pyrazole (10 and 11) or imidazole (12). For the pyrazoles, 11 is an analogue of 9 with one of the triazole nitrogens removed, whereas 10 also removes one of the triazole nitrogen atoms whilst additionally shifting the trichlorobenzophenonemethyl moiety to the 2-position equivalent.

B) H9c2 cells were treated with 3, 6 or 12 μM of CAI (9), 10, 11, 12 or the "in house" synthesised CAI in galactose containing media and after 24 hours ATP levels were measured and data shown are relative to the untreated control (n = 3). Significance was assessed using ANOVA with Dunnett's multiple comparisons test (**** $p < 0.0001$, *** $p < 0.001$, ** $p < 0.01$, * $p < 0.05$, ns = not significant).

C) Basal (i) and maximum (ii) oxygen consumption rates were measured using a Seahorse XF Analyzer in H9c2 cells treated with 3 and 10 μM of either CAI (9), 10, 11, 12 or the "in house" synthesised CAI. Error bars represent standard deviation (n = 3) and significance was assessed using ANOVA with Tukey's multiple comparisons test (**** $p < 0.0001$, *** $p < 0.001$, * $p < 0.05$).

D) A549 cells were treated with 3, 6 or 12 μM of CAI (9) or 10 and 11 in galactose containing media and after 24 hours ATP levels were measured and normalised to the untreated control. Error bars represent standard deviation (n = 3) and significance was assessed using ANOVA with Tukey's multiple comparisons test (**** $p < 0.0001$).

E) Basal and maximum oxygen consumption rates were measured using a Seahorse XF Analyzer in A549 cells treated with 5 μM of either CAI (9), 10, 11; or 5 μM mubritinib. Error

bars represent standard deviation (n = 3) and significance was assessed using ANOVA with Tukey's multiple comparisons test (**** $p < 0.0001$).

F) A549 cells were pre-treated with either 5 μM CAI (9), 10, 11, mubritinib, antimycin A or piericidin A (complex I inhibitor) and the OCR was measured over the times indicated. PMP was added to permeabilise the plasma membranes followed by addition of pyruvate, malate and ADP to drive complex I respiration and OCR determined. Finally, piericidin A was added to abolish complex I respiration followed by ADP and succinate to drive complex II respiration and OCR was again measured. Representative trace from 3 independent experiments.

G) CAI (9), 10, 11, 12 and the "in house" synthesised CAI were incubated with mitochondrial membranes at 500 nM. The rate of NADH oxidation was measured spectrophotometrically. The activity is expressed relative to the DMSO control, set to 100%. Error bars represent standard deviation (n = 3) and significance was assessed using ANOVA with Tukey's multiple comparisons test (**** $p < 0.0001$, ns = not significant). Activities were interpolated from measured data points for compounds 10, 11, 12 and "in house" CAI.

Figure 4: The toxicophore present in mubritinib and CAI is required for efficacy as an anti-cancer agent

A and B) HL60 cells grown in media containing galactose (A) or glucose (B) as an energy source treated with mubritinib (1) (2 μM), CAI (9) (5 μM) or the inactive derivatives 5 (2 μM) or 11 (5 μM) for 72 hours. The percentage of live cells was assessed by DRAQ7™ staining and Annexin-V-FITC labelling. Error bars represent standard deviation (n = 3) and significance relative to the untreated control sample was assessed using ANOVA with Dunnett's multiple comparisons test (**** $p < 0.0001$, ns = not significant).

C and D) M059K cells grown in media containing galactose (C) or glucose (D) as an energy source treated with mubritinib (1) (2 μM), CAI (9) (5 μM) or the inactive derivatives 5 (2 μM) or 11 (5 μM) for 72 hours. The percentage of live cells was assessed by DRAQ7™ staining and Annexin-V-FITC labelling. Error bars represent standard deviation (n = 3) and significance relative to the untreated control sample was assessed using ANOVA with Dunnett's multiple comparisons test (**** $p < 0.0001$, ns = not significant).

E and F) A549 cells grown in media containing galactose (E) or glucose (F) as an energy source treated with mubritinib (1) (2 μM), CAI (9) (5 μM) or the inactive derivatives 5 (2 μM) or 11 (5 μM) for 72 hours. The percentage of live cells was assessed by DRAQ7™ staining and Annexin-V-FITC labelling. Error bars represent standard deviation (n = 3) and

significance relative to the untreated control sample was assessed using ANOVA with Dunnett's multiple comparisons test (**** $p < 0.0001$, ns = not significant).

G) Cell proliferation profiles from xCELLigence RTCA DP instrument. BT474 cells grown in glucose containing media were seeded in an E-plate 16 and after 24 hours were treated with either 5 μM mubritinib (1) or the derivative compound 5 which contains a modified triazole ring. The cell index was monitored for 96 hours to determine cell proliferation rates. Error bars represent standard deviation (n = 3).

H) Cell proliferation profiles from xCELLigence RTCA DP instrument. A549 cells grown in glucose containing media were seeded in an E-plate 16 and after 20 hours were treated with either 5 μM CAI (9) or the derivative compound 11 which contains a modified triazole ring. The cell index was monitored for 120 hours to determine cell proliferation rates. Error bars represent standard deviation (n = 3).

Figure 5: Schematic diagram to show the cell-wide effect of ETC complex I inhibition by the toxicophore

Chemical inhibition of mitochondrial respiratory complex I with mubritinib and CAI leads to a decrease in cellular ATP and the subsequent activation of the energy sensor AMPK. Importantly, AMPK has been shown to phosphorylate and inhibit HER2 41, suggesting how mubritinib has been misattributed as a HER2 inhibitor, as well to negatively regulate protein synthesis via the mTOR axis to inhibit tumour cell growth. Moreover, cancer cells that are dependent on oxidative phosphorylation for ATP production, such as in AML, will be more sensitive to compounds that inhibit complex I. However, the decrease in ATP levels following treatment with these compounds will also have a particularly toxic effect on tissues with a high energy demand, such as cardiac tissue, and thus impact on heart function.

Supplementary Figure Legends

Figure 1-figure supplement 1: Mubritinib targets complex I in cardiomyocytes

A) Quantification of HER2 phosphorylation from Figure 1A displayed relative to the untreated sample. Error bars represent standard deviation (n = 3) and significance was assessed using unpaired students t-test (**** $p < 0.0001$, ** $p < 0.01$, * $p < 0.05$, ns = not significant).

B) Schematic to show the key components in the signalling pathway that is downstream from changes in energy status or inhibition of HER2. Arrows indicate activation and blocked arrows indicate inactivation of the downstream target.

C) Quantification of (i) ACC (S-79) and (ii) RPS6 (S-240/244) phosphorylation from Figure 1B displayed relative to the untreated sample. Error bars represent standard deviation (n = 3) and significance was assessed using the unpaired students t-test (* $p < 0.05$, ** $p < 0.01$, *** $p < 0.001$, ns = not significant).

Figure 2-figure supplement 1: Mubritinib inhibits OCR in H9c2 and hESC-CM

A and B) Representative seahorse trace (for Figure 2B) from (A) H9c2 or (B) hESC-CM cells in glucose containing media and treated with mubritinib (1 μM) or oligomycin A (1 μM).

Figure 2-figure supplement 2: Complex I inhibition by mubritinib and the synthesised variant compounds

A) Mubritinib and the compound variants (i-viii) were incubated with mitochondrial membranes at the concentrations shown. The rate of NADH oxidation was measured spectrophotometrically, and data were fit to the standard dose-effect relationship (activity (%) = 100 / (1 + (IC50 / [inhibitor])Hill slope). The activity is expressed relative to the DMSO control, set to 100%. For each compound the IC50 values (nM) measured on mitochondrial membranes are shown with standard errors (n = 3).

Figure 3-figure supplement 1: The toxicophore in CAI inhibits mitochondrial complex I

A and B) Representative seahorse trace (for Figure 3C) of H9c2 cells grown in glucose containing media and treated with either (A) 3 μM or (B) 10 μM of the indicated compounds.

C) A549 cells were treated with 6 or 12 μM of CAI (9) or compound 10 and compound 11 in glucose containing media and after 24 hours ATP levels were measured and normalised to the untreated control. Error bars represent standard deviation (n = 3).

D) Representative seahorse trace (for Figure 3E) of A549 cells grown in glucose containing media and treated with 5 μM of either CAI (9), 10, 11; or 5 μM mubritinib.

Figure 3-figure supplement 2: Complex I inhibition by mubritinib and the synthesised variant compounds

A) CAI and the compound variants (i-v) were incubated with mitochondrial membranes at the concentrations shown. The rate of NADH oxidation was measured spectrophotometrically, and data were fit to the standard dose-effect relationship (activity (%) = 100 / (1 + (IC50 / [inhibitor])Hill slope). The activity is expressed relative to the DMSO control, set to 100%. For each compound the IC50 values (nM) measured on mitochondrial membranes are shown with standard errors (n = 3).

Figure 3-figure supplement 3: CAI inhibits signalling pathways responsive to changes in energy status

A) Western blot analysis of A549 cells treated with 5 μM of CAI (9), 5 μM of 11 (inactive CAI derivative), 2.5 μM bepridil hydrochloride (non-specific calcium channel inhibitor) or 1 μM rotenone (complex I inhibitor) for 24 hours.
B) Quantification of (i) ACC (S-79) and (ii) RPS6 (S-240/244) phosphorylation from (E) displayed relative to the untreated sample. Error bars represent standard deviation (n = 3).

Figure 4-figure supplement 1: CAI and mubritinib inhibit cell growth and induce apoptosis in glycolytic-deficient tumour cell lines.

A and B) HL60 cells grown in media containing galactose (A) or glucose (B) as an energy source treated with mubritinib (1) (2 μM), CAI (9) (5 μM) or the inactive derivatives 5 (2 μM) or 11 (5 μM). Cells were harvested at the indicated time points and the percentage of live cells assessed by DRAQ7™staining and Annexin-V-FITC labelling. Error bars represent standard deviation (n = 3).
C and D) M059K cells grown in media containing galactose (C) or glucose (D) as an energy source treated with mubritinib (1) (2 μM), CAI (9) (5 μM) or the inactive derivatives 5 (2 μM) or 11 (5 μM). Cells were harvested at the time points shown and the percentage of live cells assessed by DRAQ7™staining and Annexin-V-FITC labelling. Error bars represent standard deviation (n = 3).
E and F) A549 cells grown in media containing galactose (E) or glucose (F) as an energy source treated with mubritinib (1) (2 μM), CAI (9) (5 μM) or the inactive derivatives 5 (2 μM) or 11 (5 μM). Cells were harvested at the time points shown and the percentage of live cells assessed by DRAQ7™staining and Annexin-V-FITC labelling. Error bars represent standard deviation (n = 3).
G) U-20S (i) cells and HeLa (ii) cells were treated with mubritinib (1) (2 μM), CAI (9) (5 μM) or the inactive derivatives compound 5 (2 μM) or compound 11 (5 μM) in media containing glucose as an energy source. Cells were harvested at the time points shown and the percentage of live cells assessed by DRAQ7™staining and Annexin-V-FITC labelling.
H) U-20S (i) cells and HeLa (ii) cells were treated with mubritinib (1) (2 μM), CAI (9) (5 μM) or the inactive derivatives compound 5 (2 μM) or compound 11 (5 μM) in media containing galactose as an energy source. Cells were harvested at the time points shown and the percentage of live cells assessed by DRAQ7™staining and Annexin-V-FITC labelling.

Supplementary Files

Supplementary File 1: Identification of compounds which contain a non-fused triazole in a conformation similar to mubritinib

ChEMBL was searched for drugs containing a non-fused triazole, which led to the identification of a number of small molecules that are used clinically either routinely or in trials use e.g. the antibiotic tazobactam, the anti-epileptic drug rufinamide, and the cancer chemotherapeutic carboxyamidotriazole. These all contain the triazole ring, but have differing associated physicochemical properties.

Supplementary File 2: Ion channel binding assay

The Ca2+ ion channel binding assay to test the activity of CAI (9), 10, 11, mubritinib (1) and 6 was performed by Eurofins. The percentage inhibition of ion channel was calculated relative to the positive control (1,4,5-IP3). On the scale used a score of 1 = no binding and a score of 100 = binding. The data show that there is no direct binding of these drugs to the ion channels.

Supplementary File 3: Ketoconazole, terconazole and rufinamide all contain a heterocyclic 1,3-nitrogen motif. The compounds listed were incubated with mitochondrial membranes and the rate of NADH oxidation was measured spectrophotometrically.

Figure 1

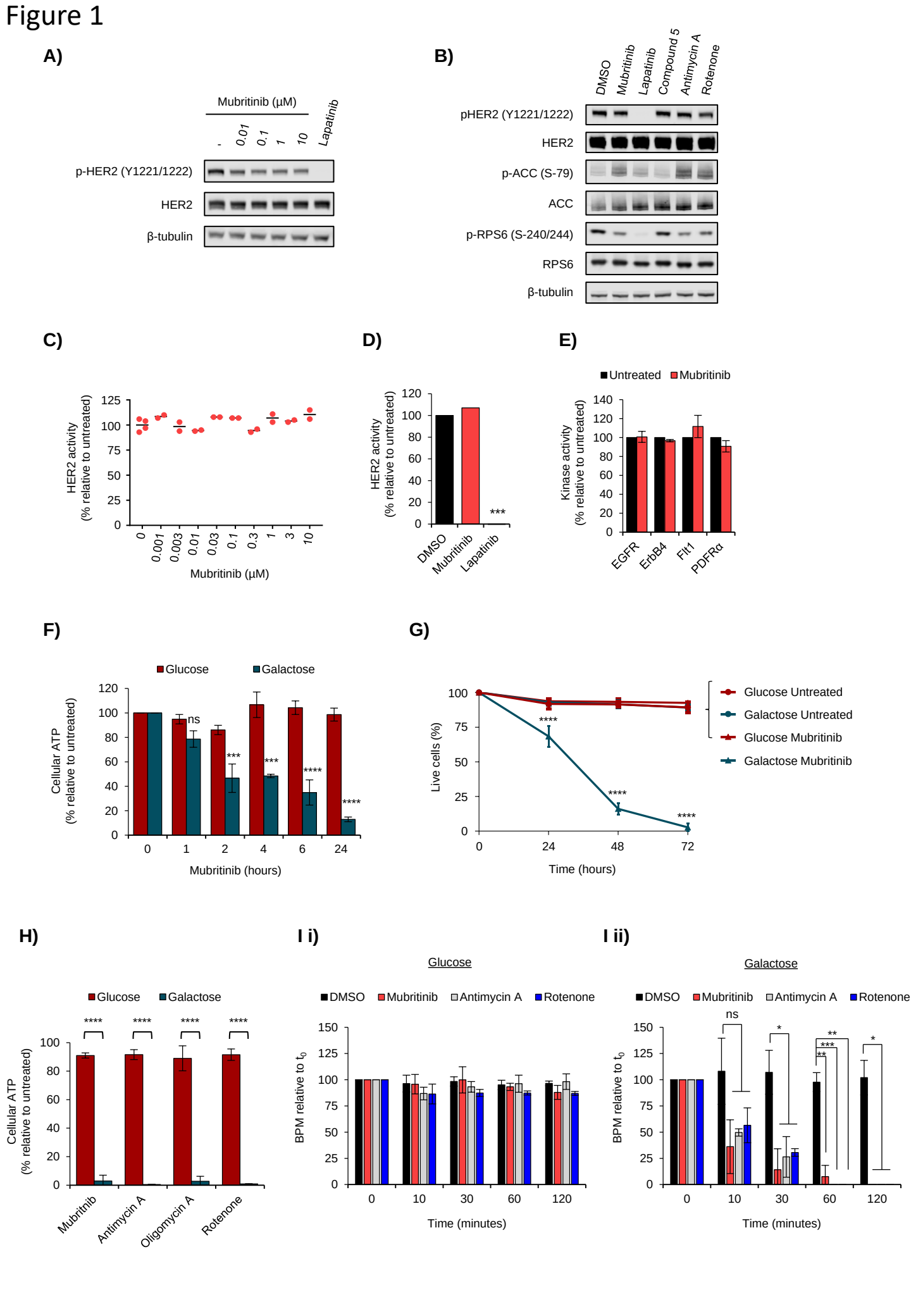
A)
Mubritinib (μM)
-
0.01
0.1
1
10
Lapatinib
p-HER2 (Y1221/1222)
HER2
β-tubulin
B)
DMSO
Mubritinib
Lapatinib
Compound 5
Antimycin A
Rotenone
pHER2 (Y1221/1222)
HER2
p-ACC (S-79)
ACC
p-RPS6 (S-240/244)
RPS6
β-tubulin
C)
HER2 activity (% relative to untreated)
Mubritinib (μM)
D)
HER2 activity (% relative to untreated)
DMSO
Mubritinib
Lapatinib
E)
Untreated
Mubritinib
Kinase activity (% relative to untreated)
EGFR
ErbB4
Flt1
PDFRα
F)
Glucose
Galactose
Cellular ATP (% relative to untreated)
Mubritinib (hours)
G)
Glucose Untreated
Galactose Untreated
Glucose Mubritinib
Galactose Mubritinib
Live cells (%)
Time (hours)
H)
Glucose
Galactose
Cellular ATP (% relative to untreated)
Mubritinib
Antimycin A
Oligomycin A
Rotenone
I i)
Glucose
DMSO
Mubritinib
Antimycin A
Rotenone
BPM relative to t0
Time (minutes)
I ii)
Galactose
DMSO
Mubritinib
Antimycin A
Rotenone
BPM relative to t0
Time (minutes)

Figure 2

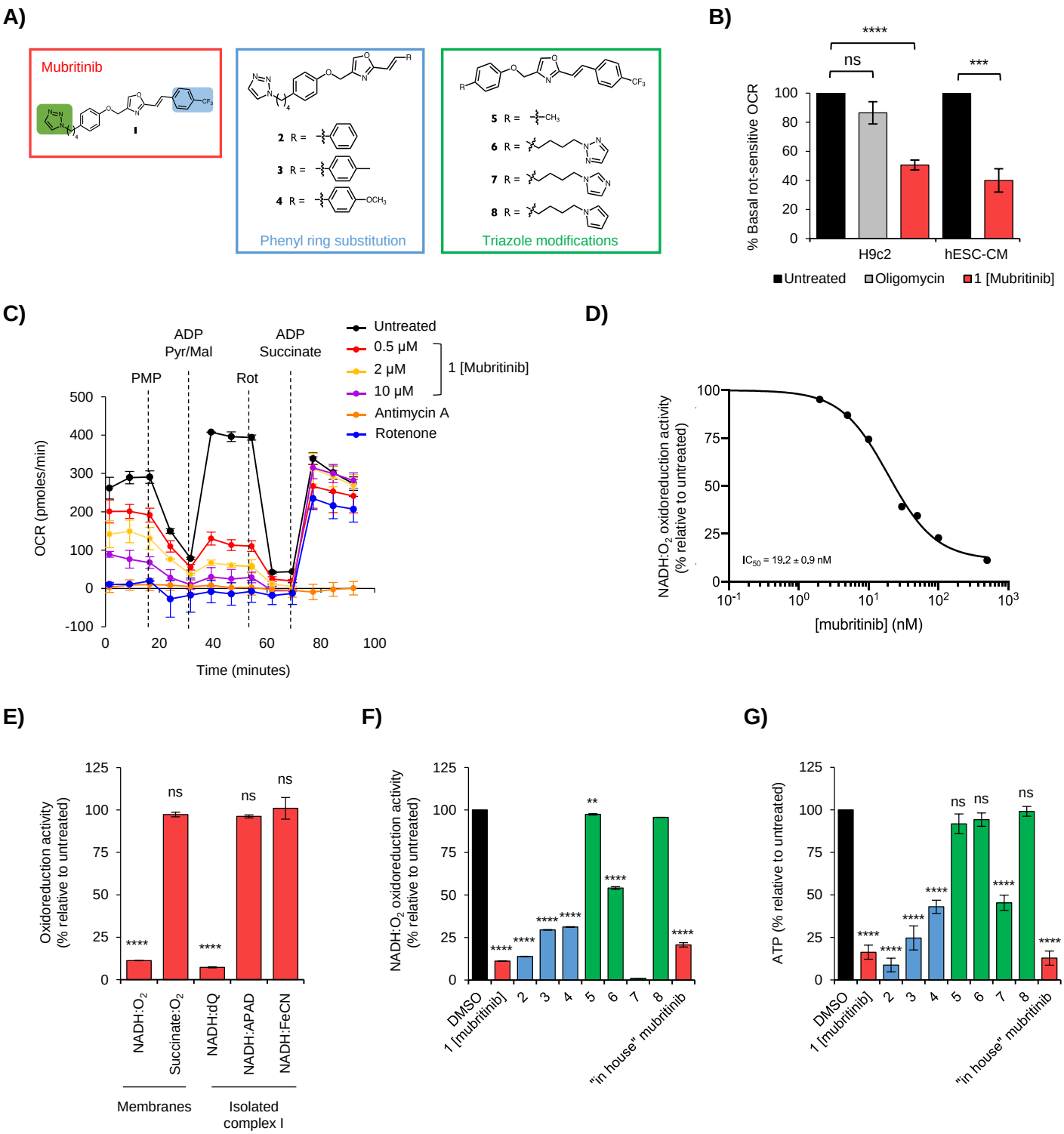
A)
Mubritinib
I
2 R =
3 R =
4 R =
Phenyl ring substitution
5 R =
6 R =
7 R =
8 R =
Triazole modifications
B)
% Basal rot-sensitive OCR
ns
****
***
H9c2
hESC-CM
Untreated
Oligomycin
1 [Mubritinib]
C)
ADP
Pyr/Mal
ADP
Succinate
PMP
Rot
Untreated
0.5 µM
2 µM
10 µM
1 [Mubritinib]
Antimycin A
Rotenone
OCR (pmoles/min)
Time (minutes)
D)
NADH:O2 oxidoreduction activity
(% relative to untreated)
IC50 = 19.2 ± 0.9 nM
[mubritinib] (nM)
E)
Oxidoreduction activity
(% relative to untreated)
NADH:O2
Succinate:O2
NADH:dQ
NADH:APAD
NADH:FeCN
Membranes
Isolated
complex I
F)
NADH:O2 oxidoreduction activity
(% relative to untreated)
DMSO
1 [mubritinib]
"in house" mubritinib
G)
ATP (% relative to untreated)
DMSO
1 [mubritinib]
"in house" mubritinib

Figure 3

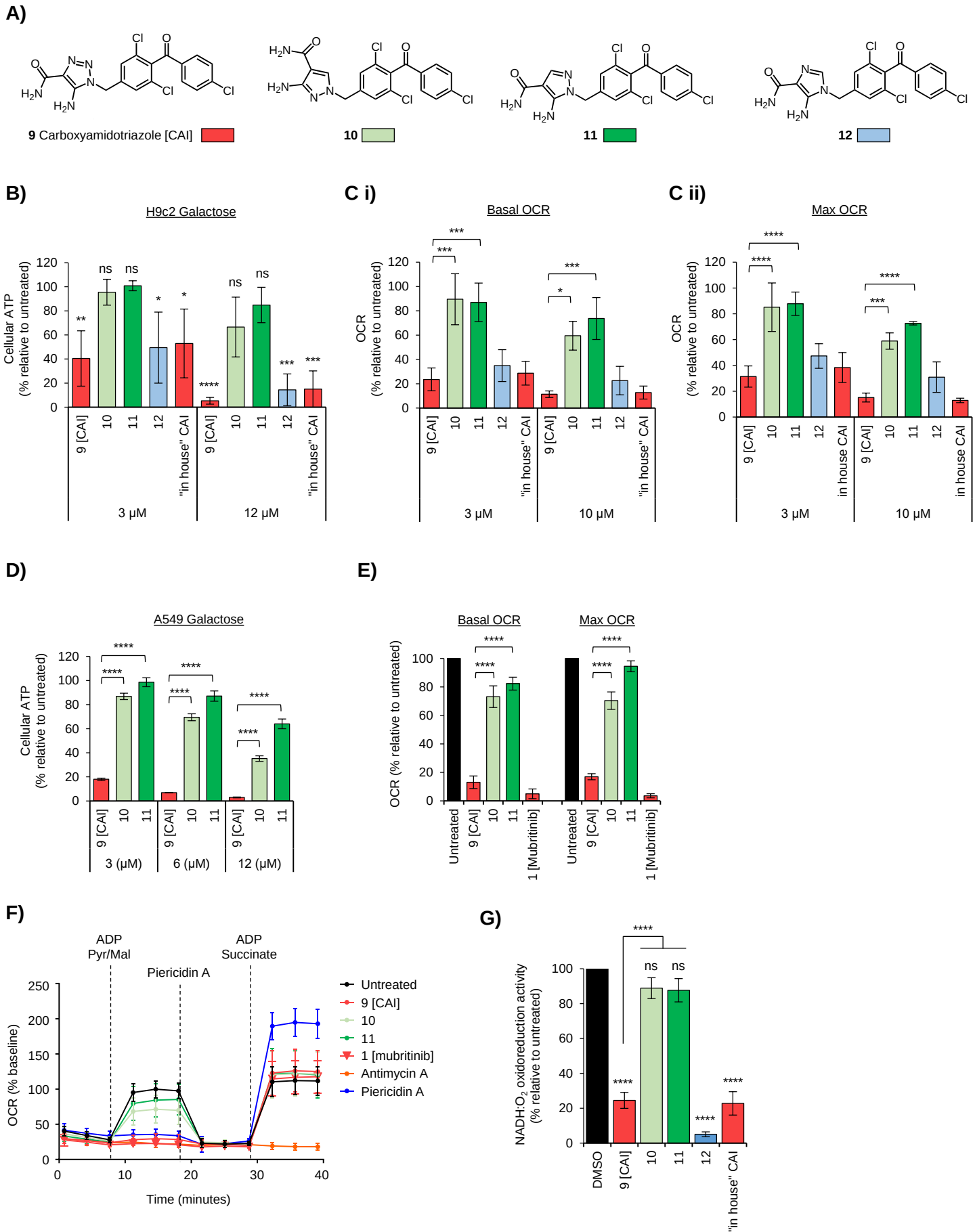
A)
9 Carboxyamidotriazole [CAI]
10
11
12
B)
H9c2 Galactose
Cellular ATP (% relative to untreated)
9 [CAI]
10
11
12
"in house" CAI
3 µM
12 µM
C i)
Basal OCR
OCR (% relative to untreated)
3 µM
10 µM
C ii)
Max OCR
in house CAI
D)
A549 Galactose
3 (µM)
6 (µM)
12 (µM)
E)
Basal OCR
Max OCR
Untreated
1 [Mubritinib]
F)
ADP Pyr/Mal
Piericidin A
ADP Succinate
OCR (% baseline)
Time (minutes)
Untreated
9 [CAI]
10
11
1 [mubritinib]
Antimycin A
Piericidin A
G)
NADH:O2 oxidoreduction activity (% relative to untreated)
DMSO
"in house" CAI

Figure 4

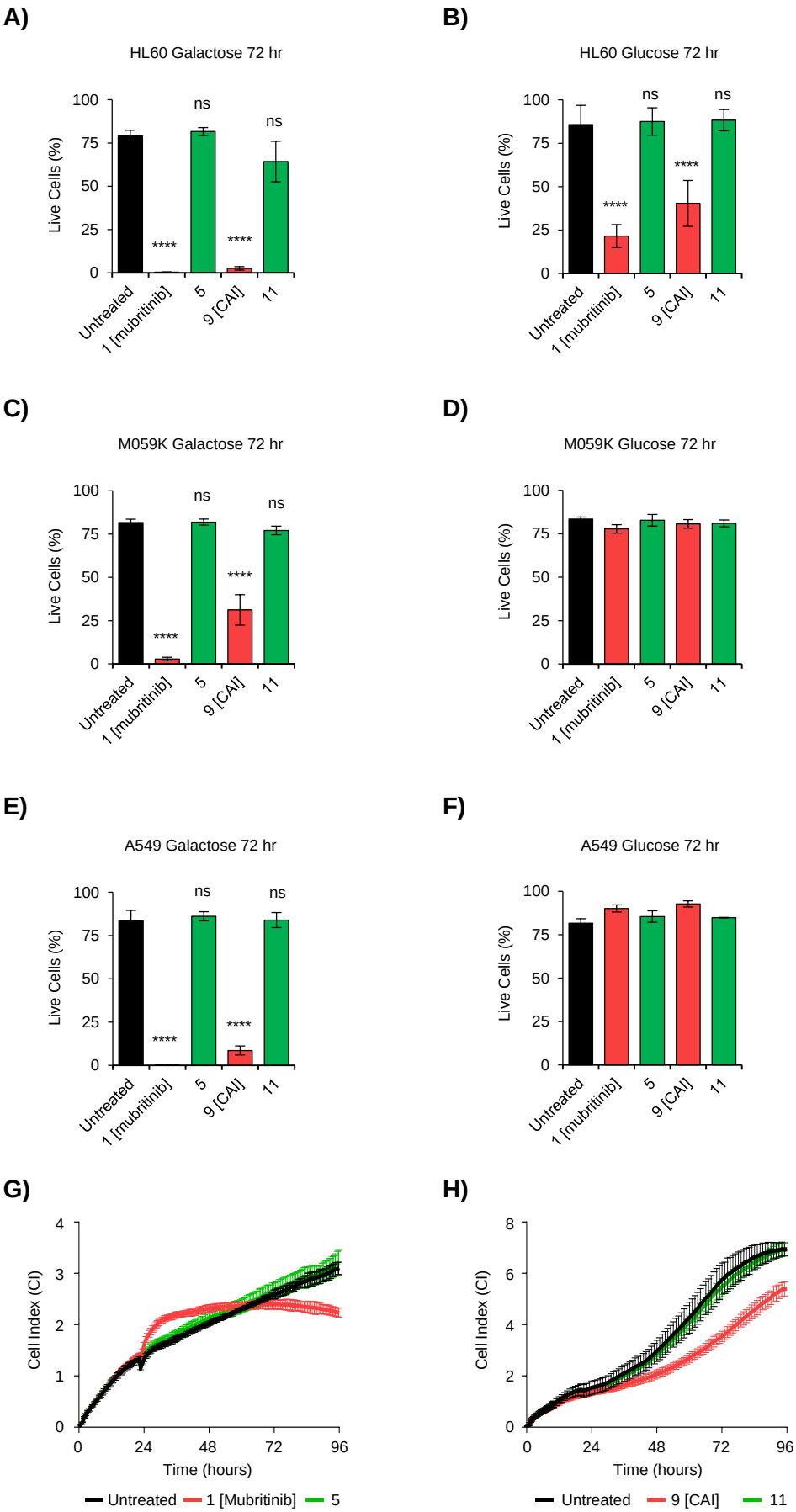
A)
HL60 Galactose 72 hr
B)
HL60 Glucose 72 hr
C)
M059K Galactose 72 hr
D)
M059K Glucose 72 hr
E)
A549 Galactose 72 hr
F)
A549 Glucose 72 hr
Live Cells (%)
100
75
50
25
0
ns
****
Untreated
1 [mubritinib]
5
9 [CAI]
11
G)
H)
Cell Index (CI)
Time (hours)
0
24
48
72
96
Untreated
1 [Mubritinib]
5
9 [CAI]
11

Figure 5

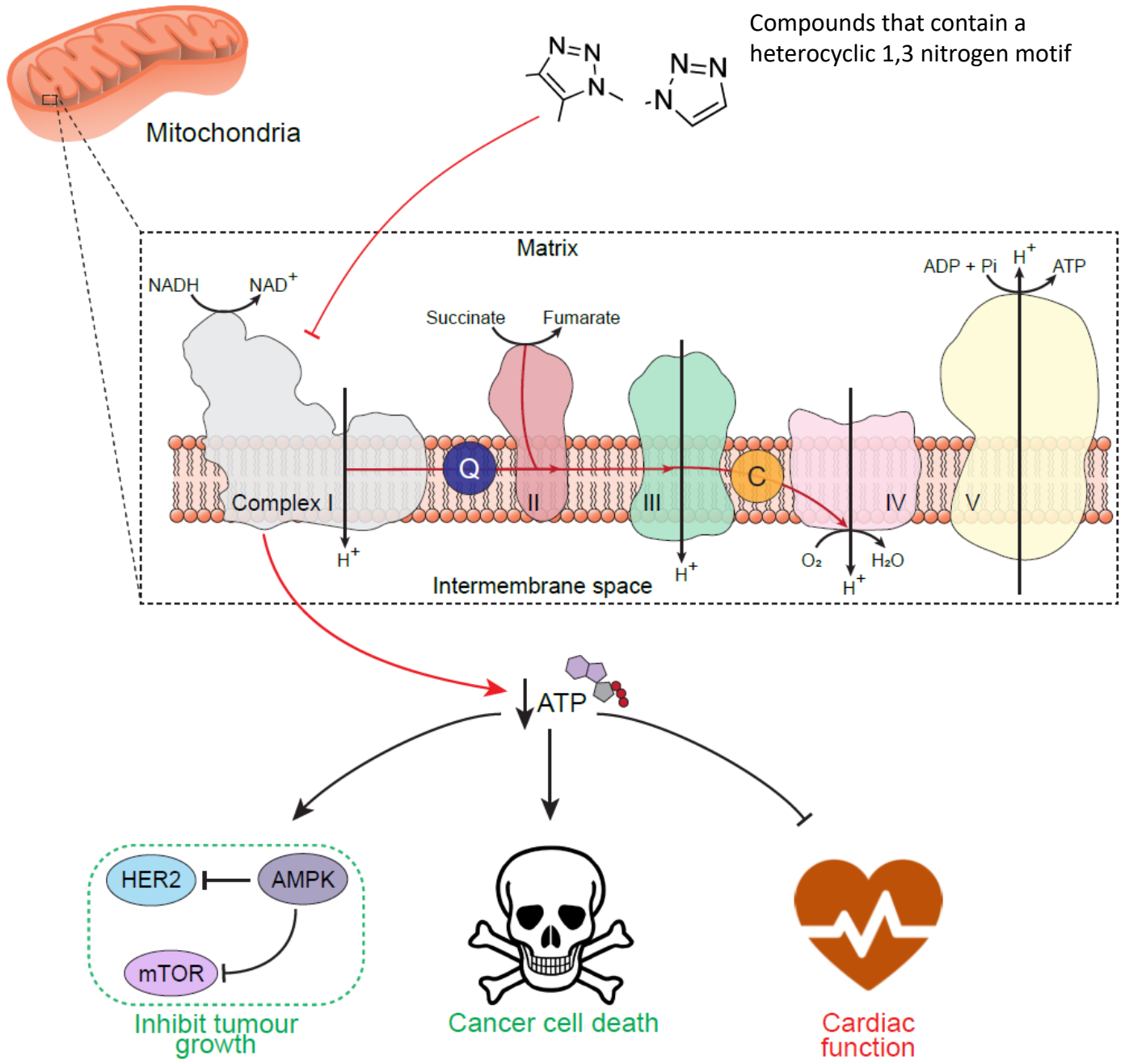
Mitochondria
Compounds that contain a heterocyclic 1,3 nitrogen motif
Matrix
NADH
NAD+
Succinate
Fumarate
ADP + Pi
H+
ATP
Q
C
Complex I
II
III
IV
V
H+
O2
H2O
Intermembrane space
ATP
HER2
AMPK
mTOR
Inhibit tumour growth
Cancer cell death
Cardiac function

Figure 1-figure supplement 1

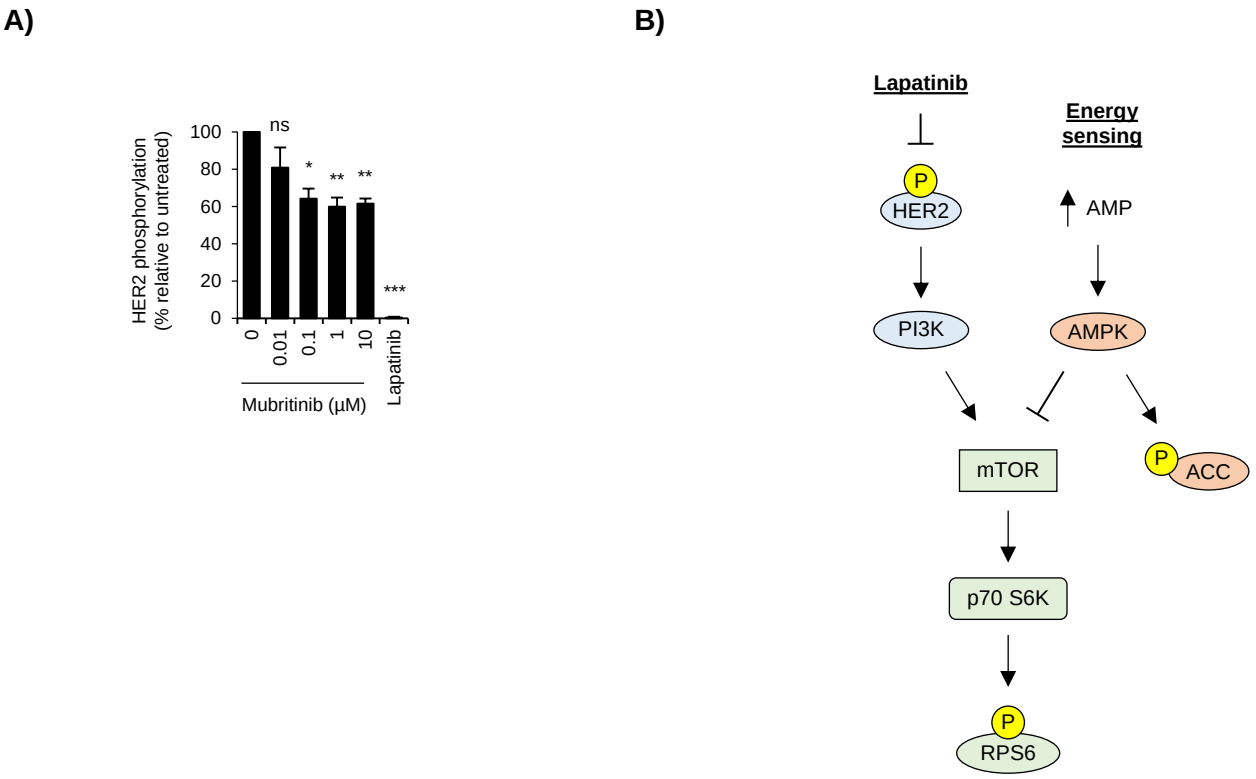

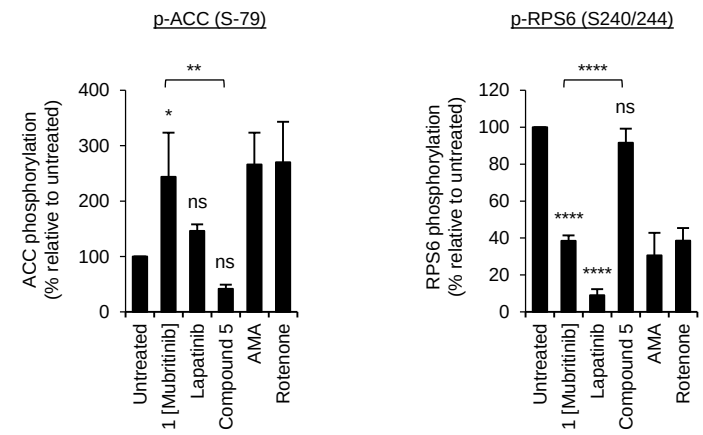

Figure 2-figure supplement 1

A)

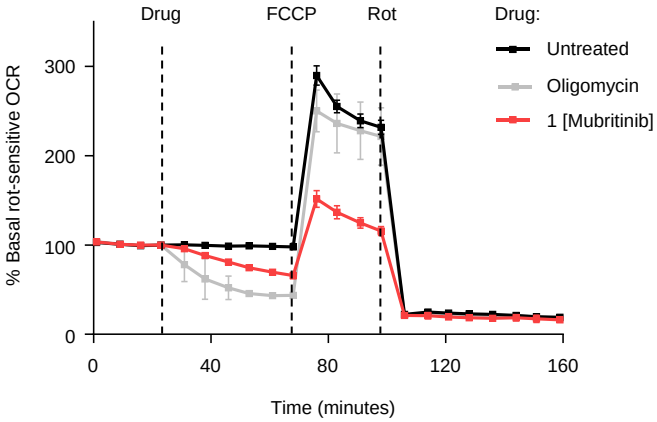

B)

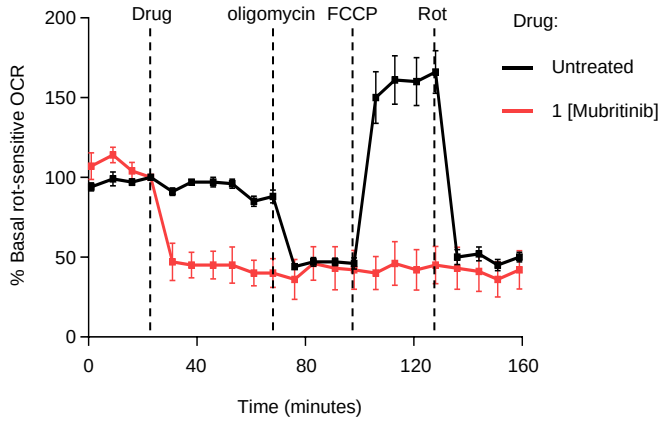

Figure 2-figure supplement 2

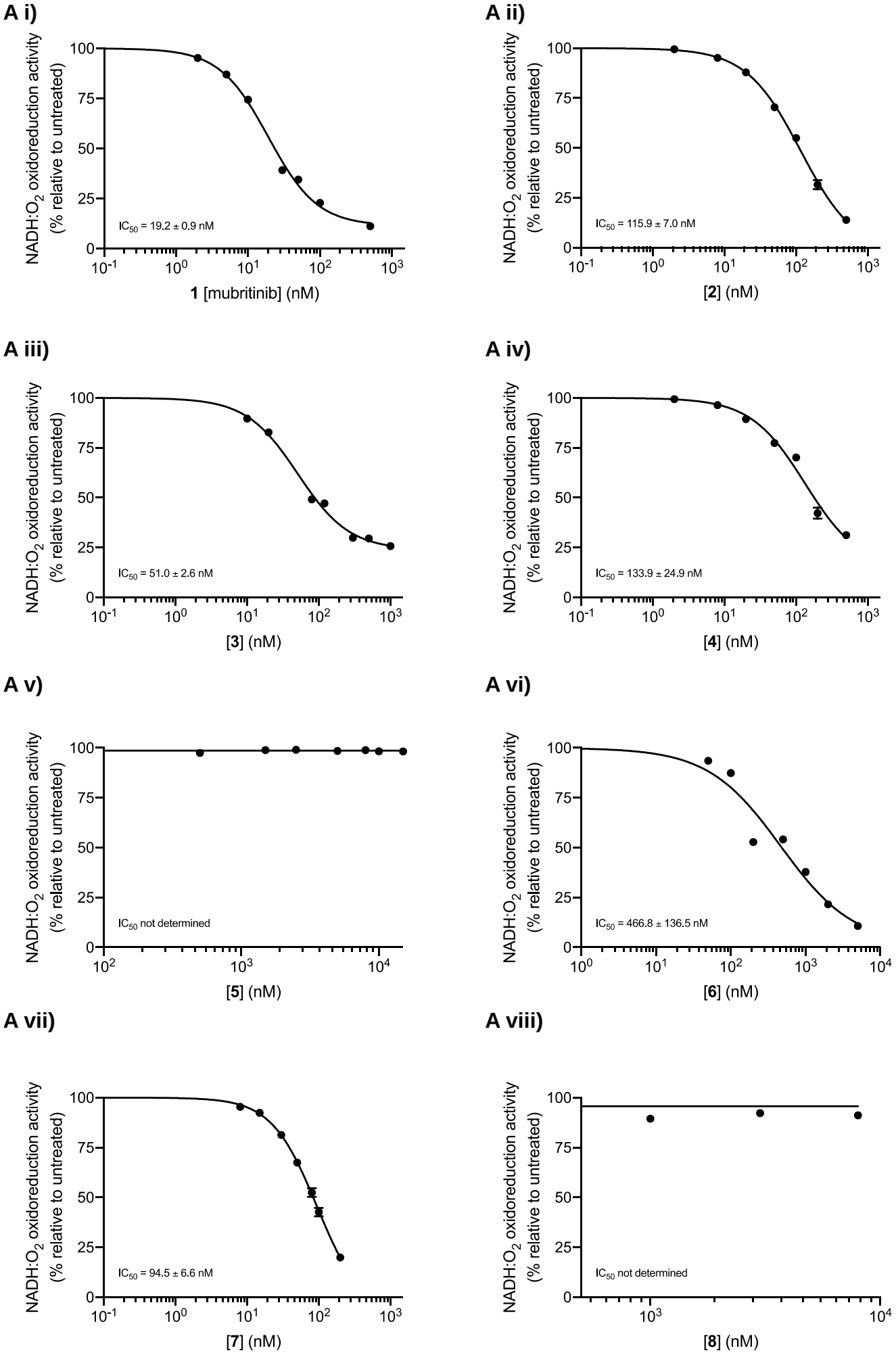

Figure 3-figure supplement 1

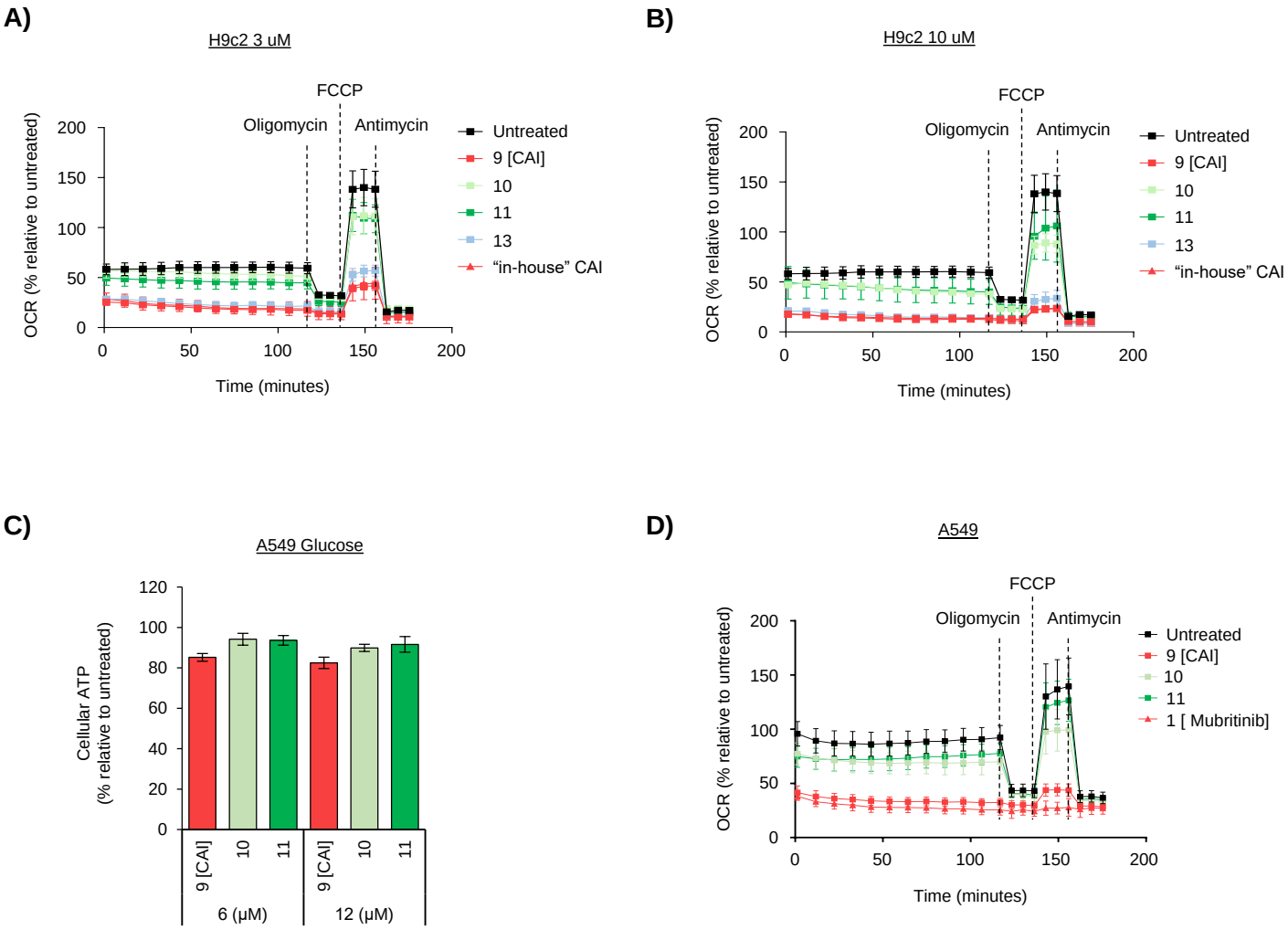

Figure 3-figure supplement 2

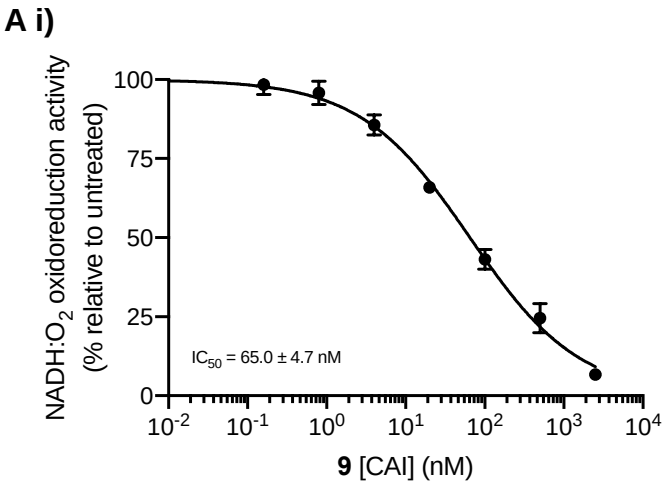

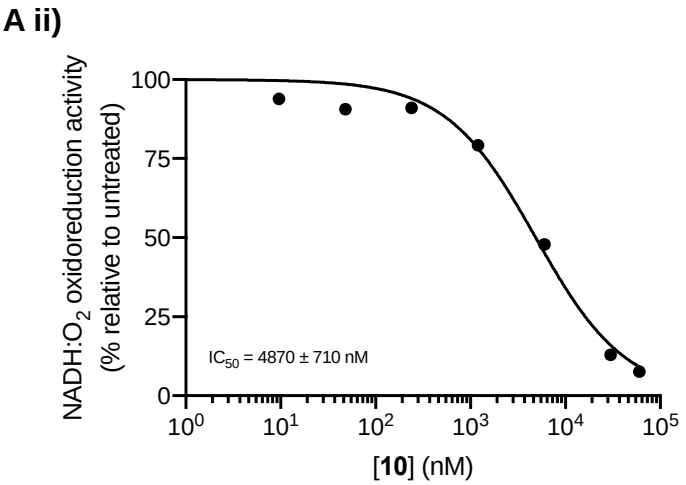

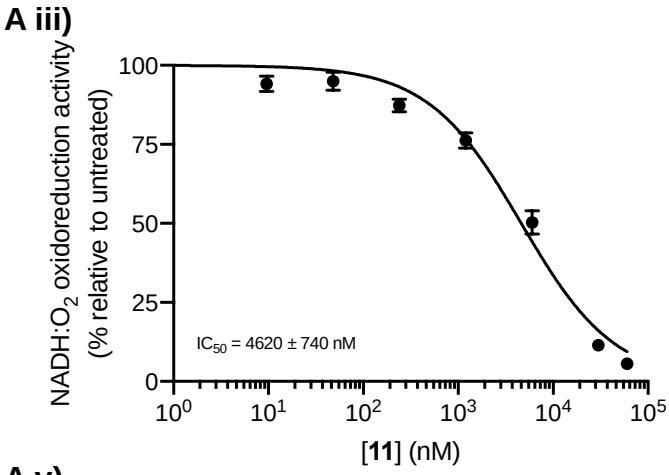

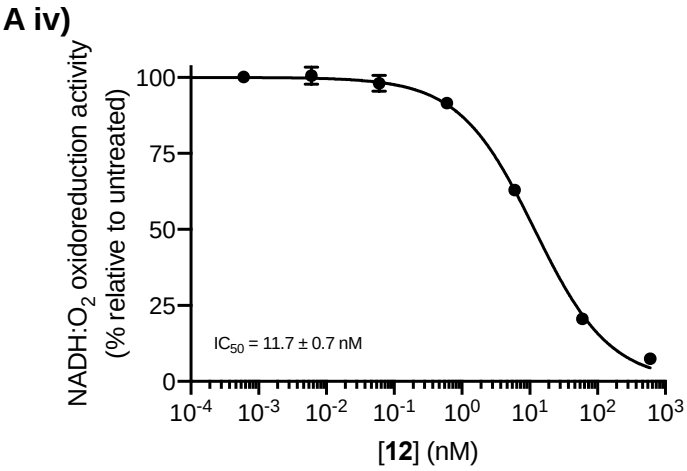

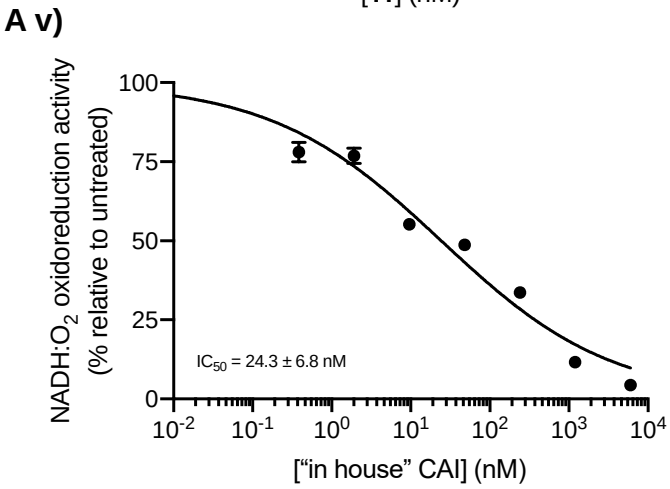

Figure 3-figure supplement 3

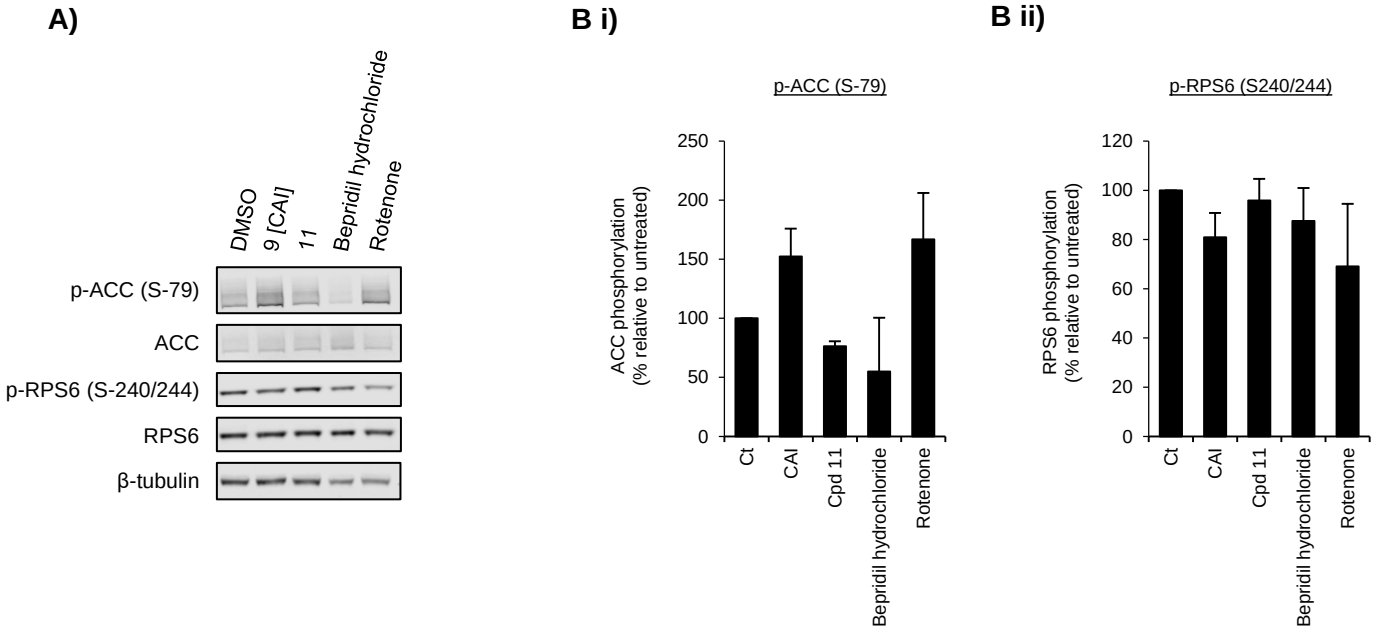

Figure 4-figure supplement 1

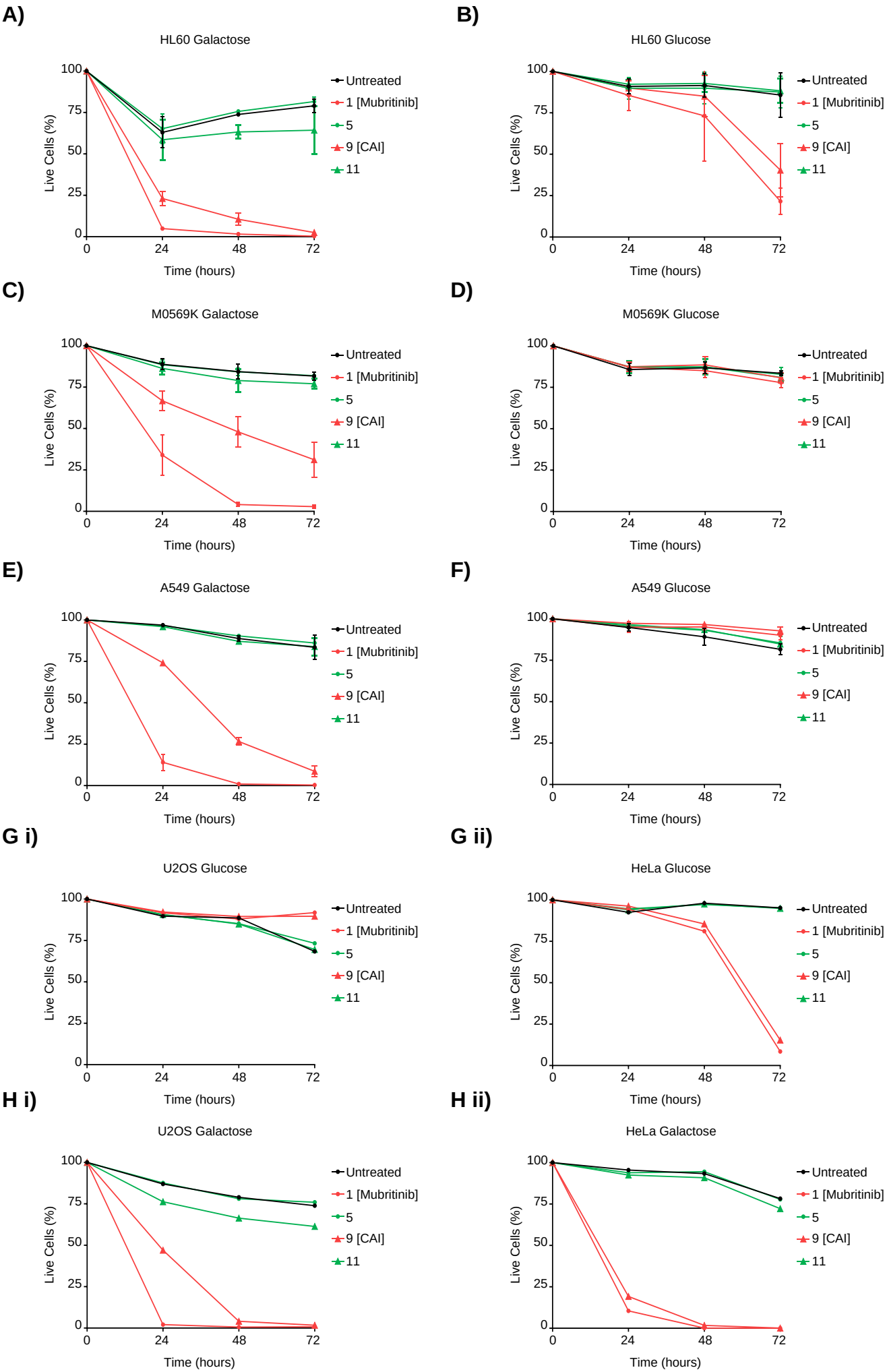

Appendix 1

Synthesis of Mubritinib and Carboxamidotriazole (CAI) Analogues

General Chemistry: Materials and Methods. Chemicals and solvents of analytical and HPLC grade were purchased from commercial suppliers and used without further purification. All reactions were carried out at ambient temperature unless otherwise stated. Reactions were monitored by thin-layer chromatography on commercially available silica pre-coated aluminium-backed plates (Merck Kieselgel 60 F254). Visualisation was under UV light (254 nm and 366 nm), followed by staining with ninhydrin or KMnO4 dips. Flash column chromatography was performed using silica gel 60, 230-400 mesh particle size (Sigma Aldrich). NMR spectra were recorded on a Bruker-AV 400. ^{1}H spectra were recorded at 400.13 Hz and ^{13}C NMR spectra at 101.62 Hz. All 13C NMR are 1H broadband decoupled. Solvents used for NMR analysis (reference peaks listed) were $CDCl_3$ supplied by Cambridge Isotope Laboratories Inc., (δH = 7.26 ppm, δC = 77.16) and CD_3OD supplied by VWR (δH = 3.31 ppm and δC = 49.00). Chemical shifts (δ) are recorded in parts per million (ppm) and coupling constants are recorded in Hz. The following abbreviations are used to described signal shapes and multiplicities; singlet (s), doublet (d), triplet (t), quartet (q), broad (br), dd (doublet of doublets), ddd (double doublet of doublets), dtd (double triplet of doublets) and multiplet (m). Spectra were assigned using appropriate COSY and HSQC experiments. Processing of the NMR data was carried out using the NMR software Topspin 3.0. LC-MS spectra were recorded on a Shimadzu UFLCXR system coupled to an Applied Biosystems API2000 and visualised at 254 nm (channel 1) and 220 nm (channel 2). LC-MS was carried out using a Phenomenex Gemini-NX C18 110A, column (50 mm × 2 mm x 3 µm) at a flow rate 0.5 mL/min over a 5 min period (Method A). All high-resolution mass spectra (HRMS) were recorded on a Bruker microTOF mass spectrometer using MS electrospray ionization operating in positive ion mode. RP-HPLC was performed on a Waters 515 LC system and monitored using a Waters 996 photodiode array detector at wavelengths between 190 and 800 nm. Spectra were analysed using Millenium 32 software. Analytical RP-HPLC was performed using a YMC-Pack C8 column (150 mm × 4.6 mm × 5 µm) and a Phenomenex Gemini NX-C18 column (250 mm × 4.6 mm × 5 µm) at a flow rate of 1.0 mL/min. Final products were one single peak and >95% pure. The retention time of the final product is reported using a gradient method of 5-95% solvent B in solvent A over 25 minutes. (Solvent A = 0.01% formic acid in H_2O, solvent B = 0.01% formic acid in CH_3CN).

Abbreviations; DCM, dichloromethane; DIAD, diisopropylazodicarboxylate; DMF, N,N-dimethylformamide; THF, tetrahydrofuran.

Mubritinib Analogues (Appendix Figure 1)

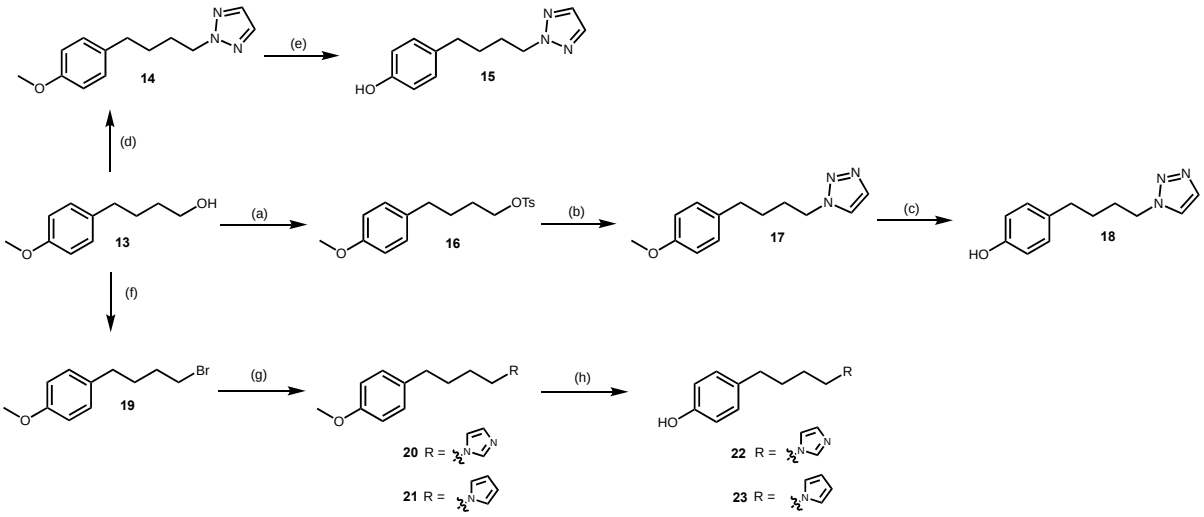

Scheme 1. *Reagents & Conditions*: (a) Tosyl chloride, triethylamine, CH_2Cl_2, 0℃ → r.t., 20 h; (b) 1*H*-1,2,3-triazole, NaOH, NaI, amyl alcohol, Δ, 5h; (c) pyridine hydrochloride, MW (180 ℃) 2 min then 6 min; (d) PPh_3, DIAD, 1*H*-1,2,3-triazole, THF, 19 h; (e) pyridine hydrochloride, MW (180 ℃) 3 x 2 min; (f) CBr_4, PPh_3, CH_2Cl_2, 18 h; (g) Imidazole, NaH, DMF, 18 h; (h) pyridine hydrochloride, MW (180 ℃) 6 min.

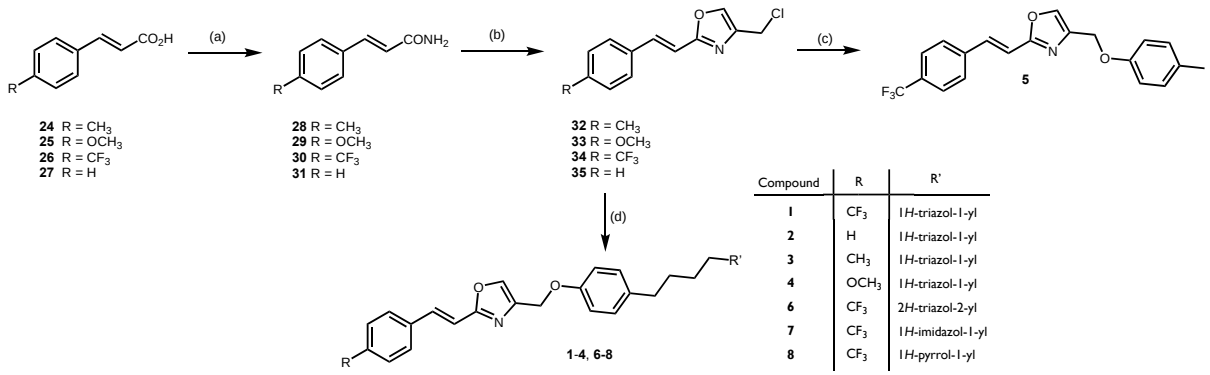

Compound	R	R'
1	CF_3	1*H*-triazol-1-yl
2	H	1*H*-triazol-1-yl
3	CH_3	1*H*-triazol-1-yl
4	OCH_3	1*H*-triazol-1-yl
6	CF_3	2*H*-triazol-2-yl
7	CF_3	1*H*-imidazol-1-yl
8	CF_3	1*H*-pyrrol-1-yl

Scheme 2. *Reagents & Conditions*: (a) (i) $(COCl_2)$, DMF, THF, (ii) NH_3, H_2O, EtOAc; (b) 1,3-dichloroacetone, toluene, Δ; (c) 4-hydroxytoluene, NaH, DMF; (d) 4-substituted phenol (cmpds **15**, **18**, **22** or **23**), NaH, DMF.

2-(4-(4-methoxyphenyl)butyl)-2*H*-1,2,3-triazole (14)

To 4-(4'-methoxyphenyl)-1-butanol (**13**) (0.20 g, 1.1 mmol, 1.0 eq) in THF (7.0 mL), triphenylphosphine (0.29 g, 1.1 mmol, 1.0 eq) was added. The mixture was stirred for 5 minutes and DIAD (0.27 g, 1.2 mmol, 1.1 eq) was then added. The solution was stirred for a further 5 minutes and 1*H*-triazole (84.0 mg, 1.2 mmol, 1.1 eq) was added. After stirring for 19 hours the THF was removed in vacuo. The residue was purified by column chromatography (1:9 EtOAc/pet. ether) to afford a pale-yellow oil (0.127 g, 49%). ^{1}H NMR (400MHz, $CDCl_3$): δ = 7.58 (s, 2H), 7.06 (d, *J* = 8.6 Hz), 6.81 (d, *J* = 8.7 Hz), 4.45 (t, *J* = 7.08 Hz, 2H), 3.78 (s, 3H), 2.58 (t, *J* = 7.71 Hz, 2H), 1.98 (quintet, *J* = 7.4 Hz, 2H), 1.64 – 1.54 (m, 2H).

^{13}C NMR (100 MHz, $CDCl_3$): δ = 157.96, 133.99, 129.37, 113.92, 55.39, 54.79, 34.39, 29.35, 28.54. LC-MS m/z calc. for $C_{13}H_{17}N_3O$ $[MH]^+$; 232.1, found; 232.2, t_R = 2.81 min.

2-(4-(4-hydroxyphenyl)butyl)-2*H*-1,2,3-triazole (15)

To a microwave vial **14** (0.51 g, 2.2 mmol, 1.0 eq) and pyridine hydrochloride (1.27 g, 1.1 mmol, 5.0 eq) were added. The mixture was heated to 180°C in the microwave for 2 minutes. This was repeated twice until all starting material was consumed. The brown solid obtained was partitioned between EtOAc and water, and the organic layer was washed a further two times with water and then dried over Na_2SO_4. The solvent was removed to afford a brown oil, which was purified by column chromatography (2:8 EtOAc/pet. ether) to afford the title compound as a dark yellow oil (0.33 g, 69%). ^{1}H NMR (400MHz, $CDCl_3$): δ = 7.59 (s, 2H), 6.99 (d, *J* = 8.5 Hz), 6.72(d, *J* = 8.5 Hz), 5.51 (s, 2H), 4.45 (t, *J* = 7.1 Hz, 2H), 2.55 (t, *J* = 7.6 Hz, 2H), 1.97 (quintet, *J* = 7.4 Hz), 1.62 – 1.52 (m, 2H). ^{13}C NMR (100 MHz, $CDCl_3$): δ = 153.9, 134.04, 133.97, 129.56, 115.34, 54.83, 34.40, 29.35, 28.53. LC-MS m/z calc. for $C_{12}H_{15}N_3O$ $[MH]^+$; 218.1, found; 218.2, t_R = 2.54 min.

4-(4-methoxyphenyl)butyl 4-methylbenzenesulfonate (16)

To 4-(4'-methoxyphenyl)-1-butanol (**13**) (2.00 g, 11.10 mmol, 1.0 eq) in $CHCl_3$ (30 mL) at 0°C, triethylamine (2.25 g, 22.2 mmol, 2.0 eq) and tosyl chloride (3.17 g, 16.6 mmol, 1.5 eq) were added. The reaction mixture was warmed to room temperature and left to stir for 20 hours. Sat. $NaHCO_3$(aq) was added and the organic layer was washed again with Sat. $NaHCO_3$(aq) and brine and then dried over $MgSO_4$. The solvent was removed *in vacuo* and the orange residue purified by column chromatography (1:9 EtOAc/pet. ether) to afford the title compound as a colourless oil (2.69 g, 72%). ^{1}H NMR (400MHz, $CDCl_3$): δ = 7.78 (d, *J* = 8.3 Hz, 1H), 7.33 (d, *J* = 7.9 Hz, 1H), 7.02 (d, *J* = 8.6 Hz, 1H), 6.80 (d, *J* = 8.6 Hz, 1H), 4.03 (t, *J* = 6.1 Hz, 1H), 3.78 (s, 3H) 2.50 (t, *J* = 7.2 Hz, 1H) 2.44 (s, 3H), 1.71-1.56 (m, 4H). ^{13}C NMR (100 MHz, $CDCl_3$): δ = 157.98, 144.79, 133.77, 133.36, 129.95, 129.36, 128.01, 113.92, 77.48, 77.36, 77.16, 76.84, 70.57, 55.40, 34.30, 28.43, 27.43, 21.77. LC-MS m/z calc. for $C_{18}H_{23}O_4S$ $[MH]^+$; 335.1, found; 335.1, t_R = 3.12 min.

1-(4-(4-methoxyphenyl)butyl)-1*H*-1,2,3-triazole (17)

To 1*H*-1,2,3-triazole (0.225 g, 3.26 mmol, 1.0 eq) in amyl alcohol (45.0 mL) NaOH (0.130 g, 3.26 mmol, 1.0 eq) and NaI (0.489 g, 3.26 mmol, 1.0 eq) were added. The mixture was heated to reflux for 1 hour and **16** (1.200 g, 3.59 mmol, 1.1 eq) in amyl alcohol (5.0 mL) was added over 10 mins. After a further 5 hours at reflux the solvent was removed and the residue partitioned between toluene and water. The organic layer was washed with sat. $NaHCO_3$(aq) and brine and dried over $MgSO_4$. The solvent was removed *in vacuo* and the crude product purified by column chromatography (1:1 EtOAc/pet.ether). The title compound was afforded as a pale-yellow oil (0.521 g, 48%). ^{1}H NMR (400 MHz, $CDCl_3$): δ 7.69 (d, *J* = 0.9 Hz, 1H), 7.50 (d, *J* = 0.9 Hz, 1H), 7.05 (d, *J* = 8.6 Hz, 2H), 6.82 (d, *J* = 8.6 Hz, 2H), 4.38 (t, *J* = 7.2 Hz, 2H), 3.78 (s, 3H), 2.59 (t, *J* = 7.5 Hz, 2H), 2.02 – 1.82 (m, 2H), 1.75 –

1.52 (m, 2H). ^{13}C NMR (101 MHz, CDCl3): δ = 158.06, 133.76, 133.56, 129.37, 123.33, 114.00, 55.40, 50.23, 34.34, 29.83, 28.47.LC-MS m/z calc. for $C_{13}H_{17}N_3O$ $[MH]^+$; 231.1, found; 231.9, t_R = 2.68 min.

1-(4-(4-hydroxyphenyl)butyl)-1*H*-1,2,3-triazole (18)

To a microwave vial **17** (0.46 g, 1.99 mmol, 1.0 eq) and pyridine hydrochloride (1.15 g, 9.94 mmol, 5.0 eq) were added. The mixture was heated to 180°C in the microwave for 6 minutes and then a further 2 minutes. The brown solid obtained was partitioned between EtOAc and water, and the organic layer was washed a further two times with water and then dried over Na_2SO_4. The solvent was removed to afford a brown oil, which was purified by column chromatography (2:98 MeOH/DCM) to afford the title compound as a pale yellow solid (0.151 g, 35 %). ^{1}H NMR (400 MHz, DMSO-d_6) δ 9.11 (s, 1H), 8.10 (d, *J* = 0.9 Hz, 1H), 7.70 (d, *J* = 0.9 Hz, 1H), 6.94 (d, *J* = 8.4 Hz, 2H), 6.65 (d, *J* = 8.4 Hz, 2H), 4.38 (t, *J* = 7.1 Hz, 2H), 2.47 (t, *J* = 7.6 Hz, 2H), 1.79 (p, *J* = 7.2 Hz, 2H), 1.44 (p, *J* = 7.7 Hz, 1H). ^{13}C NMR (101 MHz, DMSO-d_6) δ 155.29, 133.11, 131.71, 129.02, 124.56, 115.00, 48.91, 33.51, 29.33, 28.07. LC-MS m/z calc. for $C_{12}H_{15}N_3O$ $[MH]^+$; 218.1, found; 217.9, t_R = 2.39 min.

4-(4-methoxyphenyl)-1-butyl bromide (19)

To 4-(4'-methoxyphenyl)-1-butanol (**13**) (0.500 g, 2.78 mmol, 1.0 eq) and carbon tetrabromide (1.021 g, 3.05 mmol, 1.1 eq) in DCM (7.0 mL), triphenylphosphine (0.582 g, 2.22 mmol, 0.8 eq) was added. The mixture was stirred at room temperature overnight and the solvent was removed *in vacuo*. The crude orange residue was purified by column chromatography on silica (100 % pet. ether to 1:4 EtOAc/pet. ether) to afford a colourless oil (0.335 g, 50 %). ^{1}H NMR (400MHz, $CDCl_3$): δ = 7.10 (d, *J* = 8.8 Hz, 2H), 6.84 (d, *J* = 8.6 Hz, 2H), 3.79 (s, 3H), 3.42 (t, *J* = 6.7 Hz, 2H), 2.59 (t, *J* = 7.5 Hz, 2H), 1.95 – 1.83 (m, 2H), 1.82 – 1.68 (m, 2H). ^{13}C NMR (101 MHz, $CDCl_3$): δ 157.98, 134.00, 129.39, 113.94, 55.41, 34.20, 33.84, 32.36, 30.22. LC-MS m/z calc. for $C_{11}H_{15}BrO$ $[MH]^+$; 242.0, found; did not ionise, t_R = 3.23 min.

1-(4-(4-methoxyphenyl)butyl)-1*H*-imidazole (20)

To 1I-imidazole (0.134 g, 1.97 mmol, 1.0 eq) in anhydrous DMF (2.0 mL) under nitrogen and with ice cooling, sodium hydride (0.079 g, 1.97 mmol, 1.0 eq) was added. The mixture was stirred for 30 minutes and **19** (0.480 g, 1.97 mmol, 1.0 eq) in DMF (2.0 mL) was added with ice cooling. The reaction mixture was stirred for a further 18 hours and then quenched with water. The solvent was removed under vacuum and the residue purified by column chromatography on silica (5:95 MeOH/DCM) to afford the title product as a pale-yellow oil (0.310 g, 68%). ^{1}H NMR (400 MHz, $CDCl_3$): δ 7.43 (s, 1H), 7.07 – 7.02 (m, 3H), 6.87 (t, *J* = 1.3 Hz, 1H), 6.82 (d, *J* = 8.6 Hz, 2H), 3.91 (t, *J* = 7.1 Hz, 2H), 3.78 (s, 3H), 2.57 (t, *J* = 7.5 Hz, 2H), 1.85 – 1.71 (m, 2H), 1.63 – 1.53 (m, 2H). ^{13}C NMR (101 MHz, $CDCl_3$): δ 158.03, 137.16, 133.66, 129.54, 129.35, 118.88, 113.98, 55.40, 47.03, 34.48, 30.65, 28.60. LC-MS m/z calc. for $C_{14}H_{18}N_2O$ $[MH]^+$; 230.1, found; 230.8, t_R = 1.99 min.

1-(4-(4-methoxyphenyl)butyl)-1*H*-pyrrole (21)

To pyrrole (0.135 g, 2.02 mmol, 1.0 eq) in anhydrous DMF (2.0 mL) under nitrogen and with ice cooling, sodium hydride (0.081 g, 2.02 mmol, 1.0 eq) was added. The mixture was stirred for 30 minutes and **19** (0.490 g, 1.97 mmol, 1.0 eq) in DMF (2.0 mL) was added with ice cooling. The reaction mixture was stirred for a further 18 hours and then quenched with water. The solvent was removed under vacuum and the residue was purified by column chromatography on silica (5:95 MeOH/DCM) to afford the title product as a colourless oil (0.189 g, 41%). ^{1}H NMR (400 MHz, $CDCl_3$): δ 7.07 (d, *J* = 8.7 Hz, 2H), 6.83 (d, *J* = 8.6 Hz, 2H), 6.64 (t, *J* = 2.1 Hz, 2H), 6.14 (t, *J* = 2.1 Hz, 2H), 3.88 (t, *J* = 7.1 Hz, 2H), 3.80 (s, 3H) 2.57 (t, *J* = 7.6 Hz, 2H), 1.89 – 1.74 (m, 2H), 1.67 – 1.56 (m, 2H). ^{13}C NMR (101 MHz, $CDCl_3$): δ 157.93, 134.13, 129.39, 120.59, 113.90, 107.97, 55.40, 49.62, 34.64, 31.19, 28.86. LC-MS m/z calc. for $C_{15}H_{19}NO$ $[MH]^+$; 229.1, found; 230.1, t_R = 3.15 min.

1-(4-(4-hydroxyphenyl)butyl)-1*H*-imidazole (22)

To a microwave vial **20** (0.21 g, 0.89 mmol, 1.0 eq) and pyridine hydrochloride (0.51 g, 4.45 mmol, 5.0 eq) were added. The mixture was heated to 180°C in the microwave for 6 minutes. The brown solid obtained was partitioned between EtOAc and water. The organic layer was washed twice with water and then dried over Na_2SO_4. As some product remained in the aqueous layer it was basified to pH8 and re-extracted with EtOAc. The solvent was removed to afford a brown solid, which was purified by column chromatography (5:95 MeOH/DCM) to afford the title compound as a white solid (98.6 mg, 51%). ^{1}H NMR (400 MHz, $CDCl_3$): δ = 7.47 (s, 1H), 7.07 (s, 1H), 6.95 (d, *J* = 8.4 Hz, 2H), 6.88 (s, 1H), 6.79 (d, *J* = 8.5 Hz, 2H), 3.92 (t, *J* = 7.0 Hz, 2H), 2.54 (t, *J* = 7.4 Hz, 2H), 1.79 (p, *J* = 7.1 Hz, 2H), 1.55 (p, *J* = 7.6 Hz, 2H). ^{13}C NMR (101 MHz, $CDCl_3$): δ = 155.62, 136.80, 132.34, 129.37, 128.74, 119.12, 115.74, 77.48, 77.36, 77.16, 76.84, 47.26, 34.49, 30.41, 28.55. LC-MS m/z calc. for $C_{13}H_{17}N_2O$ $[MH]^+$; 217.2, found, 217.3 t_R = 1.02 min.

1-(4-(4-hydroxyphenyl)butyl)-1*H*-pyrrole (23)

To a microwave vial **21** (0.14 g, 0.61 mmol, 1.0 eq) and pyridine hydrochloride (0.35 g, 3.05 mmol, 5.0 eq) were added. The mixture was heated to 180°C in the microwave for 6 minutes. The brown solid obtained was partitioned between EtOAc and water, and the organic layer was washed twice with water and then dried over Na_2SO_4. The solvent was removed to afford a brown oil, which was purified by column chromatography (1:9 to 2:8 EtOAc/pet. ether) to afford the title compound as a colourless oil (81.9 mg, 63%). ^{1}H NMR (400MHz, $CDCl_3$): δ = 7.01 (d, *J* = 8.7 Hz, 1H), 6.74 (d, *J* = 8.5 Hz, 1H), 6.64 (t, *J* = 2.1 Hz, 2H), 6.14 (t, *J* = 2.1 Hz, 2H), 3.87 (t, *J* = 7.1 Hz, 2H), 2.55 (t, *J* = 7.6 Hz, 2H), 1.84-1.73 (m, 2H), 1.61 – 1.53 (m, 2H). ^{13}C NMR (100 MHz, $CDCl_3$): δ = 153.76, 134.27, 129.57, 120.60, 115.29, 107.98, 77.47, 77.36, 77.16, 76.84, 49.61, 34.64, 31.16, 28.84. m/z calc. for $C_{14}H_{18}NO$ $[MH]^+$; 216.2, found; 216.1, t_R = 2.89.

Synthesis of propenamides (28-31)

***General method A* with (*E*)-3-phenyl-2-propenamide (31) as an example.**

To *trans*-cinnamic acid (**27**) (1.0 g, 6.8 mmol, 1.0 eq) in THF (10 mL) at 0°C under nitrogen, DMF (1 drop) and oxalyl chloride (1.0 g, 8.1 mmol, 1.2 eq) were added. The mixture was stirred at room temperature for 2 hours and further oxalyl chloride (0.5 eq) was added. The solvent was removed *in vacuo* and the resulting oil dissolved in EtOAc (5 mL) and added dropwise to a stirred mixture of 35% NH_4OH(aq) (5.0 mL) and EtOAc (2.0 mL) at 0°C. The resulting white needle-like crystals were recovered by vacuum filtration and washed with water and petroleum ether to afford the title compound (0.891 g, 90%). ^{1}H NMR (400MHz, DMSO-d_6): δ = 7.59 – 7.52 (m, 3H), 7.47 - 7.33 (m, 4H), 7.13 (broad s, 1H), 6.62 (d, *J* = 15.9 Hz, 1H). ^{13}C NMR (100 MHz, DMSO-d_6): δ = 166.68, 139.15, 134.88, 129.42, 128.90, 127.52, 122.34. LC-MS m/z calc. for C_9H_9NO $[MH]^+$; 148.1, found; 148.1, t_R = 2.18 min.

(*E*)-3-(4-methylphenyl)-2-propenamide (28)

Compound **28** was prepared according to the procedure described in general method A using (*E*)-3-(p-tolyl)acrylic acid (**24**) as starting material. White solid (0.831 g, 84%). ^{1}H NMR (400MHz, DMSO-d_6): δ = 7.51 (broad s, 1H), 7.45 (d, *J* = 8.1 Hz, 2H), 7.38 (d, *J* = 15.9 Hz, 1H), 7.21 (d, *J* = 7.9 Hz, 2H), 7.08 (broad s, 1H), 6.56 (d, *J* = 15.9 Hz, 1H), 2.31 (s, 3H). ^{13}C NMR (100 MHz, DMSO-d_6): δ = 166.83, 139.15, 139.09, 132.13, 129.49, 127.79, 121.29, 20.91. LC-MS m/z calc. for $C_{10}H_{12}NO$ $[MH]^+$; 162.1, found; 162.2, t_R = 2.35 min.

(*E*)-3-(4-methoxyphenyl) propenamide (29)

Compound **29** was prepared according to the procedure described in general method A using (*E*)-3-(4-methoxyphenyl)acrylic acid (**25**) as starting material. White solid (0.833 g, 84%). ^{1}H NMR (400MHz, DMSO-d_6): δ = 7.49 (d, *J* = 8.8 Hz, 2H), 7.46 (broad s, 1H), 7.37 (d, *J* = 15.8 Hz, 1H), 7.01 (broad s, 1H), 6.96 (d, *J* = 8.8 Hz, 2H), 6.47 (d, *J* = 15.9 Hz 1H), 3.78 (s, 3H). ^{13}C NMR (100 MHz, DMSO-d_6): δ = 167.00, 160.31, 138.88, 129.09, 127.43, 119.81, 114.36, 55.23. LC-MS m/z calc. for $C_{10}H_{11}NO_2$ $[MH]^+$; 178.1, found; 178.2, t_R = 2.21 min.

(*E*)-3-(4-trifluoromethylphenyl)-2-propenamide (30)

Compound **30** was prepared according to the procedure described in general method A using (*E*)-3-(4-trifluoromethylphenyl)acrylic acid (**26**) as starting material. White solid (0.850 g, 85%). ^{1}H NMR (400MHz, DMSO-d_6): δ = 7.72 (m, 4H), 7.63 (broad s, 1H), 7.49 (d, *J* = 15.9 Hz, 1H), 7.24 (broad s, 1H), 6.75 (d, *J* = 15.9 Hz, 1H). ^{13}C NMR (100 MHz, DMSO-d_6): δ = 166.18, 138.97, 129.20 (q, *J* = 31.8 Hz), 128.14, 125.74 (q, *J* = 3.8 Hz), 125.18, 122.73 (q, *J* = 272.1 Hz). LC-MS m/z calc. for $C_{10}H_9F_3NO$ $[MH]^+$; 216.0, found; 216.2, t_R = 2.62 min.

Synthesis of oxazole intermediates (32-35)

***General method B* with 4-chloromethyl-2-[(*E*)-2-phenylethenyl]-oxazole (35) as an example.**

To **31** (0.500g, 3.39 mmol, 1.0 eq) in toluene (5.0 mL), 1,3-dichloroacetone (0.431g 3.39 mmol, 1.0 eq) was added. The mixture was stirred at reflux for 4.5 hours and after cooling was poured onto sat. K_2CO_3(aq). The aqueous layer was extracted with EtOAc and the combined organic layers were washed with water, brine, and then dried over Na_2SO_4. The crude product was then purified by column chromatography (1:9 EtOAc/pet. ether) to afford the title product as a white crystalline solid (0.323g, 43%). ^{1}H NMR (400MHz, $CDCl_3$): δ = 7.62 (s, 1H), 7.58–7.50 (m, 3H), 7.43–7.31 (m, 3H), 6.92 (d, *J* = 16.37, 1H), 4.54 (d, *J* = 0.8 Hz, 2H). ^{13}C NMR (100 MHz, $CDCl_3$): δ = 162.49, 139.14, 137.43, 136.10, 135.61, 129.76, 129.26, 127.62, 113.79, 37.34. LC-MS m/z calc. for $C_{12}H_{11}{}^{35}ClNO$ $[MH]^+$; 220.1, found; 220.1, t_R = 2.88 min.

4-chloromethyl-2-[(*E*)-2-(4-methylphenyl)ethenyl]-1,3-oxazole (32)

Compound **32** was prepared according to the procedure described in general method B using **28** as starting material. A further 0.5 eq of 1,3-dichloroacetone was added after 24 hours. Column chromatography eluent; 1:9 EtOAc/pet. ether. The title compound was obtained as a white solid (0.444 g, 61%). ^{1}H NMR (400MHz, $CDCl_3$): δ = 7.61 (s, 2H), 7.51 (d, *J* = 16.4 Hz, 1H), 7.42 (d, J = 8.1 Hz, 2H), 7.19 (d, J = 8.0 Hz, 2H), 6.87 (d, J = 16.4 Hz, 1H), 4.53 (d, *J* = 0.8 Hz, 2H), 2.37 (s, 3H). ^{13}C NMR (100 MHz, $CDCl_3$): δ = 162.51, 139.83, 138.84, 137.21, 135.74, 132.67, 129.77, 127.34, 112.56, 37.18, 21.53. LC-MS m/z calc. for $C_{13}H_{13}{}^{35}ClNO$ $[MH]^+$; 234.1 found; 234.4, t_R = 3.09 min.

4-chloromethyl-2-[(*E*)-2-(4-methoxyphenyl)ethenyl]-1,3-oxazole (33)

Compound **33** was prepared according to the procedure described in general method B using **29** as starting material. Column chromatography eluent; 1:9 EtOAc/pet. ether. The title compound was obtained as a pale yellow solid (0.238 g, 34%). ^{1}H NMR (400 MHz, $CDCl_3$) δ 7.60 (s, 1H), 7.51 (s, 1H), 7.49 (d, *J* = 16.3 Hz 7.47 (d, *J* = 8.5 Hz, 1H), 6.92 (d, *J* = 8.8 Hz, 2H), 6.78 (d, *J* = 16.4 Hz, 1H), 4.53 (d, *J* = 1.0 Hz, 2H), 3.84 (s, 3H). ^{13}C NMR (100 MHz, $CDCl_3$): δ =162.56, 161.03, 138.95, 137.02, 135.77, 129.07, 128.36, 114.69, 111.52, 55.69, 37.39. LC-MS m/z calc. for $C_{13}H_{13}{}^{35}ClNO_2$ $[MH]^+$; 250.0, found; 250.2, t_R = 2.85 min.

4-chloromethyl-2-[(*E*)-2-(4-trifluoromethylphenyl)ethenyl]-1,3-oxazole (34)

Compound **34** was prepared according to the procedure described in general method B using **30** as starting material. Column chromatography eluent; 1:9 EtOAc/pet. ether. The title compound was obtained as a white solid (0.359 g, 54%). ^{1}H NMR (400MHz, $CDCl_3$): δ = 7.68 – 7.59 (m, 5H), 7.56 (d, *J* = 7.6 Hz, 1H), 6.99 (d, *J* = 16.4 Hz, 1H), 4.54 (d, *J* = 0.8 Hz, 2H). ^{13}C NMR (100 MHz, $CDCl_3$): δ = 161.63, 139.25, 138.79, 136.33, 135.39, 131.28, 130.95, 127.51, 126.04 (q, *J* = 3.9 Hz), 124.07 (q, *J* = 272.24), 115.94, 37.00, LC-MS: m/z calc. for $C_{13}H_{10}{}^{35}ClF_3NO$ $[MH]^+$; 288.04, found; 287.9, t_R = 3.16 min.

4-(4'-methylphenoxymethyl)-2-[(E)-2-(4-trifluoromethylphenyl)ethenyl]-1,3-oxazole (**5**)
To a solution of **34** (0.12 g, 0.42 mmol, 1.0 eq) in DMF (5.0 mL), sodium hydride (60% in mineral oil, 17.0 mg, 0.42 mmol, 1.0 eq) was added under N_2 with ice cooling. The mixture was stirred at room temperature for 30 minutes and *p*-cresol (45.0 mg, 0.42 mmol, 1.0 eq) was added. The mixture was stirred at room temperature for 23 hours and water (20 mL) was then added. A precipitate formed which was isolated by vacuum filtration, washed with water and petroleum ether and was then purified by column chromatography (1:9 EtOAc/pet. ether). The solvent was removed in vacuo to afford the title compound as a white crystalline solid. ^{1}H NMR (400MHz, $CDCl_3$): 7.67 (s, 1H), 7.67 – 7.59 (m, 4H), 7.54 (d, *J* = 16.5 Hz, 1H), 7.10 (d, *J* = 8.3 Hz, 2H), 7.01 (d, *J* = 16.4 Hz, 1H), 6.89 (d, *J* = 8.6 Hz, 2H), 5.02 (d, *J* = 0.98, 2H), 2.29 (s, 3H) ^{13}C NMR (100 MHz, $CDCl_3$): δ = 161.38, 156.33, 139.03, 138.94, 136.57, 134.92, 130.93 (q, *J* = 29.1 Hz), 130.12, 127.47, 126.02 (q, *J* = 3.9 Hz), 121.41 (q, *J* = 270.9 Hz), 116.18, 114.81, 62.83, 20.64. HRMS: (m/z) calc for $C_{20}H_{16}F_3NO_2$ $[MH]^+$; 360.1206 found; 360.1213. LC-MS m/z calc. for $C_{20}H_{16}F_3NO_2$ $[MH]^+$; 360.1, found; 360.2, t_R = 3.35 min. Analytical RP-HPLC t_R = 22.35, 95% purity.

Synthesis of triazole, pyrrole and imidazole final compounds (1-4 & 6-8)

***General method C* with (*E*)-4-((4-(4-(2*H*-1,2,3-triazol-2-yl)butyl)phenoxy)methyl)-2-(4-(trifluoromethyl)styryl)oxazole (6) as an example**

To a solution of **15** (30.0 mg, 0.14 mmol, 1.0 eq) in DMF (2.0 mL), sodium hydride (60% in mineral oil, (55.0 mg, 0.14 mmol, 1.0 eq) was added with ice cooling under N_2. The mixture was stirred at room temperature for 30 minutes and **34** (39.0 mg, 0.14 mmol, 1.0 eq) was added with ice cooling. The mixture was stirred at room temperature for 19 hours and water was then added. A precipitate formed which was isolated by vacuum filtration and was then purified by column chromatography (2:8 EtOAc/pet. ether). The title compound was obtained as a white solid (20.0 mg, 31%). ^{1}H NMR (400MHz, $CDCl_3$): δ = 7.67 (s, 1H), 7.66 – 7.59 (m, 4H), 7.54 (d, *J* = 16.3 Hz, 1H) 7.58 (s, 1H), 7.08 (d, *J* = 8.6 Hz, 2H), 7.01 (d, *J* = 16.4 Hz, 1H), 6.91 (d, *J* = 8.6 Hz, 2H), 5.02 (s, 1H), 5.01 (s, 1H), 4.46 (t, *J* = 7.0 Hz, 2H), 2.59 (t, *J* = 7.6 Hz, 2H), 1.99 (quintet, *J* = 7.4 Hz, 2H), 1.65 – 1.54 (m, 2H). ^{13}C NMR (100 MHz, $CDCl_3$): δ = 161.25, 156.56, 138.86, 138.79, 136.44, 134.79, 134.63, 133.89, 130.88 (q, J = 31.1 Hz), 129.34, 127.34, 125.88 (q, *J* = 3.8 Hz), 123.96 (q, *J* = 271.6 Hz), 116.05, 114.73, 62.67, 54.66, 34.31, 29.24, 28.36. HRMS: (m/z) calc. for $C_{25}H_{23}N_4O_2$ $[MH]^+$; 469.1846 found; 469.1849. LC-MS m/z calc. for $C_{25}H_{23}N_4O_2$ $[MH]^+$; 469.2, found; 469.2, t_R = 3.21 min. Analytical RP-HPLC: t_R = 22.26, Purity = 99%.

(*E*)-4-((4-(4-(1*H*-1,2,3-triazol-1-yl)butyl)phenoxy)methyl)-2-((4-trifluoromethyl)styryl)oxazole (1)

Compound **1** was prepared according to the procedure described in general method C using compounds **18** and **34** as starting materials**.** Column chromatography eluent (1:1 EtOAc/pet. ether) the title compound was obtained as a white solid (39.0 mg, 60%). ^{1}H NMR (400 MHz,

DMSO-d_6):) δ 8.24 (s, 1H), 8.11 (d, *J* = 0.9 Hz, 1H), 7.95 (d, *J* = 8.1 Hz, 2H), 7.76 (d, *J* = 8.2 Hz, 2H), 7.70 (d, *J* = 0.9 Hz, 1H), 7.61 (d, *J* = 16.4 Hz, 1H), 7.34 (d, *J* = 16.5 Hz, 1H), 7.09 (d, *J* = 8.6 Hz, 2H), 6.94 (d, *J* = 8.6 Hz, 2H), 4.98 (d, *J* = 0.9 Hz, 2H), 4.39 (t, *J* = 7.1 Hz, 2H), 2.54 (d, *J* = 7.6 Hz, 2H), 1.81 (m, 2H), 1.60 – 1.39 (m, 2H). ^{13}C NMR (101 MHz, DMSO-d_6):) δ = 160.55, 156.18, 139.19, 138.11, 138.08, 134.30, 134.07, 133.12, 129.18, 128.05, 125.63 (q, *J* = 3.4 Hz), 124.58, 124.11 (q, *J* = 271.8), 116.42, 114.55, 61.49, 48.88, 33.44, 29.32, 27.96. LC-MS *m/z* calc. for $C_{25}H_{23}N_4O_2$ $[MH]^+$; 469.2, found; 469.1, t_R = 3.09 min. HRMS: (m/z) calc. for $C_{25}H_{23}N_4O_2$ $[MH]^+$; 469.1846 found; 469.1853. Analytical RP-HPLC: t_R = 20.19 min, purity = 99%.

(*E*)-4-((4-(4-(1*H*-1,2,3-triazol-1-yl)butyl)phenoxy)methyl)-2-(styryl)oxazole (2)

Compound **2** was prepared according to the procedure described in general method C using compounds **18** and **35** as starting materials**.** Column chromatography eluent; 7:3 EtOAc/pet. ether. The title compound was obtained as an off-white solid (0.05 g, 68%). ^{1}H NMR (400 MHz, $CDCl_3$) δ 7.71 (s, 1H), 7.65 (s, 1H), 7.61 – 7.46 (m, 4H), 7.44 – 7.31 (m, 3H), 7.07 (d, *J* = 8.3 Hz, 2H), 6.95 (d, *J* = 16.5 Hz, 1H), 6.92 (d, *J* = 8.5 Hz, 2H), 5.02 (s, 2H), 4.39 (t, *J* = 7.1 Hz, 2H), 2.60 (t, *J* = 7.5 Hz, 2H), 1.94 (m, 2H), 1.63 (m, 2H). ^{13}C NMR (101 MHz, $CDCl_3$) δ = 162.08, 156.79, 138.14, 137.63, 136.27, 135.34, 134.29, 133.59, 129.68, 129.49, 129.07, 127.51, 123.61, 114.99, 113.28, 62.65, 50.48, 34.39, 29.84, 28.43. LC-MS *m/z* calc. for $C_{24}H_{24}N_4O_2$ $[MH]^+$; 401.2, found; 401.1, t_R = 3.02 min. HRMS: (m/z) calc. for $C_{24}H_{24}N_4O_2$ $[MH]^+$; 401.1972 found; 401.1976. Analytical RP-HPLC t_R = 18.99 min, purity = 98%.

(*E*)-4-((4-(4-(1*H*-1,2,3-triazol-1-yl)butyl)phenoxy)methyl)-2-((4-methyl)styryl)oxazole (3)

Compound **3** was prepared according to the procedure described in general method C using **18** and **32** as starting materials. Column chromatography eluent; 8:2 EtOAc/pet. ether. The title compound was obtained as a white solid (38.0 mg, 50%). ^{1}H NMR (400 MHz, $CDCl_3$): δ 7.70 (s, 1H), 7.64 (s, 1H), 7.53 (d, *J* = 16.4 Hz, 1H), 7.50 (s, 1H), 7.43 (d, *J* = 8.0 Hz, 2H), 7.20 (d, *J* = 7.9 Hz, 2H), 7.07 (d, *J* = 8.6 Hz, 2H), 6.91 (d, *J* = 8.6 Hz, 1H), 6.89 (d, *J* = 16.4 Hz, 1H), 5.01 (d, *J* = 1.1 Hz, 2H), 4.39 (t, *J* = 7.2 Hz, 2H), 2.60 (t, *J* = 7.5 Hz, 2H), 2.38 (s, 3H), 2.05 – 1.87 (m, 2H), 1.75 – 1.52 (m, 2H). ^{13}C NMR (101 MHz, $CDCl_3$): δ = 162.30, 156.79, 140.05, 137.97, 137.77, 136.11, 134.30, 133.66, 132.59, 129.80, 129.47, 127.50, 123.45, 114.98, 112.17, 62.61, 50.35, 34.38, 29.83, 28.42, 21.58. LC-MS *m/z* calc. for $C_{25}H_{26}N_4O_2$ $[MH]^+$; 415.2, found; 415.1, t_R = 3.08 min. HRMS: (m/z) calc. for $C_{25}H_{26}N_4O_2$ $[MH]^+$; 415.2129 found; 415.2132. Analytical RP-HPLC t_R = 19.68 min, purity = 97%.

(*E*)-4-((4-(4-(1H-1,2,3-triazol-1-yl)butyl)phenoxy)methyl)-2-((4-methoxy)styryl)oxazole (4)

Compound **4** was prepared according to the procedure described in general method C using **18** and **33** as starting materials. Column chromatography eluent; (8:2 EtOAc/pet. ether) the title compound was obtained as a white solid (48.4 mg, 81%). ^{1}H NMR (400 MHz, CDCl3): δ 7.69 (d, *J* = 1.0 Hz, 1H), 7.62 (s, 1H), 7.50 (d, *J* = 16.6 Hz, 1H), 7.49 (d, *J* = 1.0 Hz, 1H), 7.48 (d, *J* = 8.6 Hz, 2H), 7.06 (d, *J* = 8.6 Hz, 2H), 6.92 (d, *J* = 8.8 Hz, 2H), 6.91 (d, *J* = 8.6 Hz, 2H), 6.80

(d, *J* = 16.4 Hz, 1H), 5.00 (d, *J* = 1.1 Hz, 2H), 4.39 (t, *J* = 7.2 Hz, 2H), 3.84 (s, 3H), 2.60 (t, *J* = 7.5 Hz, 2H), 1.97-1.90 (m, 2H), 1.67 – 1.56 (m, 2H). 13C NMR (101 MHz, CDCl3): δ 162.47, 160.97, 156.78, 137.87, 137.36, 135.93, 134.30, 133.80, 129.46, 129.04, 128.09, 123.11 (q, *J* = 271.8 Hz) 123.35, 114.95, 114.54, 110.90, 62.61, 55.54, 50.25, 34.39, 29.85, 28.43. LC-MS m/z calc. for $C_{25}H_{23}N_4O_2$ $[MH]^+$; 431.2, found; 431.0, t_R = 3.00 min. HRMS: (m/z) calc. for $C_{25}H_{23}N_4O_2$ $[MH]^+$; 431.2078 found; 431.2079. Analytical RP-HPLC: t_R = 18.83 min, purity = 99%.

(*E*)-4-((4-(4-(1*H*-imidazol-1-yl)butyl)phenoxy)methyl)-2-(4-(trifluoromethyl)styryl)oxazole (7)

Compound **7** was prepared according to the procedure described in general method C using **22** and **34** as starting materials**.** Column chromatography eluent; 3:7 EtOAc/pet ether. The title compound was obtained as a white solid (61.8 mg, 95%). ^{1}H NMR (400MHz, $CDCl_3$): δ = 7.68 (br s, 1H), 7.67-7.59 (m, 4H), 7.55 (d, *J* = 16.5 Hz, 1H), 7.44 (br s, 1H)7.06 (d, *J* = 8.6 Hz, 2H), 7.04 (br s, 1H) 7.01 (d, *J* = 16.4 Hz, 1H), 6.92 (d, *J* = 8.7 Hz, 3H), 6.87 (br s, 1H), 5.02 (d, *J* = 1.0 Hz, 2H), 3.92 (t, *J* = 7.1 Hz, 2H), 2.58 (t, *J* = 7.5 Hz, 2H), 1.79 (m, 2H), 1.59 (m, 2H). ^{13}C NMR (100 MHz, $CDCl_3$): δ = 161.40, 156.77, 138.88, 137.16, 136.59, 134.97, 134.43, 129.52, 129.44, 127.46, 126.00 (q, *J* = 3.6 Hz), 118.89, 116.13, 114.92, 77.47, 77.36, 77.15, 76.84, 62.76, 47.04, 34.51, 30.64, 28.54. HRMS: (m/z) calc. for $C_{26}H_{24}F_3N_3O_2$ $[MH]^+$; 468.1893 found; 468.1914. LC-MS *m/z* calc. for $C_{26}H_{24}F_3N_3O_2$ $[MH]^+$; 468.2, found; 468.3, t_R = 2.50 min. Analytical RP-HPLC: t_R = 17.64, purity = 97%.

(*E*)-4-((4-(4-(1*H*-pyrrol-1-yl)butyl)phenoxy)methyl)-2-(4-(trifluoromethyl)styryl)oxazole (8)

Compound **8** was prepared according to the procedure described in general method C using **23** and **34** as starting materials**.** Column chromatography eluent; 1:9 to 2:8 EtOAc/pet ether. The title compound was obtained as an off-white solid (55.1 mg, 85%). ^{1}H NMR (400MHz, $CDCl_3$): δ = 7.68 (s, 1H), 7.64 (m, 4H), 7.55 (d, *J* = 16.4 Hz, 1H), 7.08 (d, *J* = 8.6 Hz, 2H), 7.02 (d, *J* = 16.4 Hz, 1H), 6.91 (d, *J* = 8.6 Hz, 1H), 6.63 (t, *J* = 2.1 Hz, 2H), 6.13 (t, *J* = 2.1 Hz, 2H), 5.02 (d, *J* = 1.1 Hz, 2H), 3.87 (t, *J* = 7.1 Hz, 2H), 2.57 (t, *J* = 7.6 Hz, 2H), 1.88 – 1.71 (m, 2H), 1.65 – 1.57 (m, 1H). ^{13}C NMR (100 MHz, $CDCl_3$): δ = 161.39, 156.67, 138.97, 136.58, 134.95, 134.91, 129.49, 127.47, 126.02 (q, *J* = 3.6 Hz), 120.60, 116.17, 114.85, 108.00, 77.48, 77.36, 77.16, 76.84, 62.80, 49.62, 34.68, 31.19, 28.80. HRMS: (m/z) calc. for $C_{27}H_{25}F_3N_2O_2$ $[MH]^+$; 467.1941 found; 467.1944. LC-MS *m/z* calc. for $C_{27}H_{25}F_3N_3O_2$ $[MH]^+$; 467.2, found; 467.5, t_R = 3.48 min. Analytical RP-HPLC: t_R = 23.23, purity = 97%.

Carboxamidotriazole (CAI) Analogues

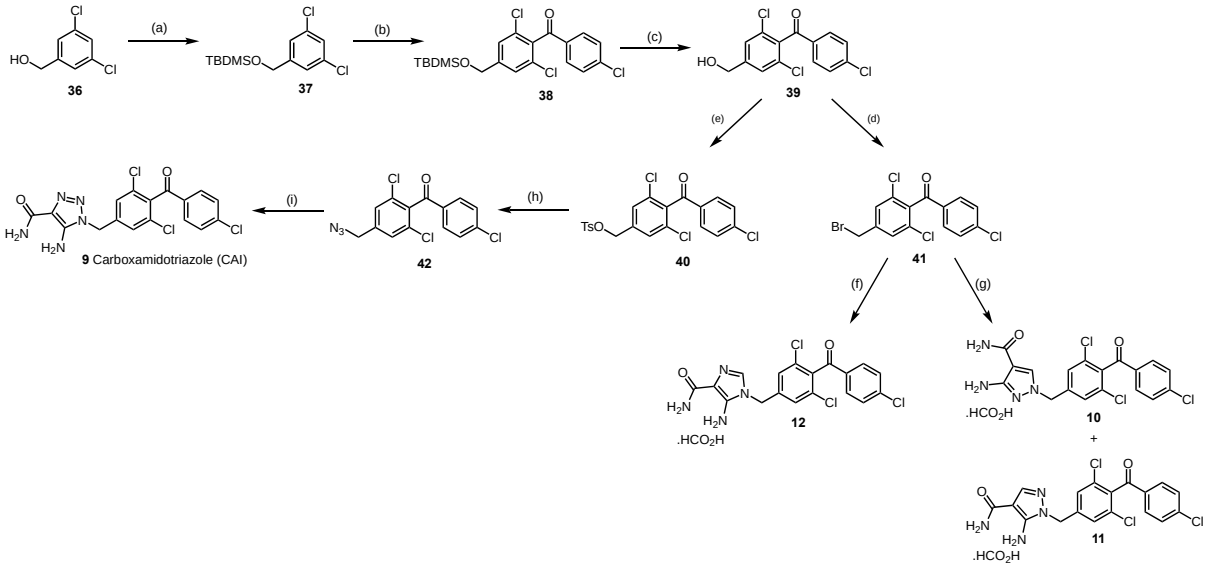

Scheme 3. *Reagents & Conditions:* (a) TBDMSCl, imidazole, DMAP, DMF; (b) (i) *n*BuLi, THF, -78 °C, 4-chlorobenzoyl chloride; (c) TBAF, THF; (d) PBr_3, THF; (e) Tosyl chloride, DIPEA, $CHCl_3$; (f) 5-amino-1*H*-imidazole-4-carboxamide, K_2CO_3, MeCN; (g) 3-aminopyrazole-carboxamide, NaH, DMF; (h) NaN_3, EtOH (i) Cyanoacetamide, EtOH, 30% NaOMe in MeOH.

tert-butyl((3,5-dichlorobenzyl)oxy)dimethylsilane (37)

To a mixture of 3,5-dibromobenzyl alcohol (**36**) (3.00 g, 16.9 mmol) and imidazole (2.77 g, 40.7 mmol) in DMF (30 mL), was added *tert*-butyldimethylsilyl chloride (3.06 g, 20.3 mmol). After stirring for 1 day at room temperature, the mixture was diluted with ether, washed twice with water and then dried over $MgSO_4$. Concentration of the organic phase afforded a clear colourless oil (4.94 g, 100%) ^{1}H NMR (400 MHz, Chloroform-*d*) δ 7.25 – 7.22 (m, 1H), 7.21 – 7.18 (m, 2H), 4.68 (s, 2H), 0.95 (s, 9H), 0.11 (s, 6H). ^{13}C NMR (101 MHz, $CDCl_3$) δ 145.12, 134.93, 127.10, 124.44, 63.88, 26.04, 18.53, -5.18.

(4-(((*tert*-butyldimethylsilyl)oxy)methyl)-2,6-dichlorophenyl)(4-chlorophenyl)methanone (38)

A mixture of **37** (1.00 g, 3.4 mmol) in anhydrous THF (10 mL) was cooled to -72°C in a hexane/dry ice bath. *n*-Butyl lithium (2.3M, 1.5 mL, 3.8 mmol) was added dropwise keeping the temperature ≤-60°C. The mixture was stirred at ≤60°C for 30 minutes and was then cooled to -72°C. Chlorobenzoyl chloride (0.52 mL, 4.1 mmol) in THF (2 mL) was added dropwise keeping the temperature below -60°C. The mixture was stirred at -60°C for 3 hours and was then quenched with 2M $HCl_{(aq)}$ (2 mL) and allowed to warm to room temperature. The THF was removed under vacuum and the residue was partitioned between EtOAc and water. The organic layer was washed with sat. $NaHCO_3$, brine and then dried over $MgSO_4$. The solvent was removed to afford a pale-yellow oil containing small crystals. The crude product was loaded onto isolute and purified by column chromatography (100% pet. ether to 20% DCM). The solvent was removed to afford a pale yellow oil (0.500g, 34%). ^{1}H NMR (400 MHz, Chloroform-*d*) δ 7.76 (d, *J* = 8.6 Hz, 2H), 7.45 (d, *J* = 8.6 Hz, 2H), 7.34 (s, 2H), 4.75 (t, *J* = 0.9 Hz, 2H), 0.97 (s, 9H), 0.14 (s, 6H). ^{13}C NMR (101 MHz, $CDCl_3$) δ 191.68, 145.76, 140.96, 135.58,

134.16, 131.86, 131.10, 129.48, 125.52, 63.60, 26.04, 18.55, -5.17. LC-MS *m/z* calc. for $C_{20}H_{24}Cl_3O_2Si$ $[MH]^+$; 429.1, found; 429.1, t_R = 3.78 min.

(4-Chlorophenyl)(2,6-dichloro-4-(hydroxymethyl)phenyl)methanone (39)

To a solution of **38** (0.50 g, 1.2 mmol) in THF (8 mL), TBAF (1M in THF, 2.1 mL, 2.1 mmol) was added. The mixture was stirred for 5hrs at room temperature. EtOAc was added and the solution washed twice with sat. $NH_4Cl_{(aq)}$ and then water. The organic phase was dried over $MgSO_4$, filtered and the solvent was removed to afford a white solid. The solid was triturated with pet. ether and collected by vacuum filtration. (0.282 g, 77%). ^{1}H NMR (400 MHz, Chloroform-*d*) δ 7.76 (d, *J* = 8.6 Hz, 2H), 7.46 (d, *J* = 8.6 Hz, 2H), 7.39 (s, 2H), 4.76 (d, *J* = 4.4 Hz, 2H), 2.06 (t, *J* = 5.8 Hz, 1H). ^{13}C NMR (101 MHz, $CDCl_3$) δ 191.60, 144.93, 141.09, 136.11, 134.03, 132.12, 131.09, 129.52, 126.18, 63.63. LC-MS *m/z* calc. for $C_{14}H_{10}Cl_3O_2$ $[MH]^+$; 315.0, found; 315.1, t_R = 2.92 min.

3,5-dichloro-4-(4'-chlorobenzoyl)benzyl 4''-methylbenzenesulfonate (40)

To **39** (0.20 g, 0.63 mmol) in chloroform (3 mL) at 0°C, DIPEA (0.22 mL, 1.27 mmol) and tosyl chloride (0.18 g, 0.95 mmol) were added. The mixture was allowed to warm to room temperature and was stirred for 24 hrs. 0.5 equivalents (0.06g, 0.32 mmol) of tosyl chloride were added and the mixture was stirred for a further 24hrs. Sat. $NaHCO_3$ and chloroform were added, and the organic layer was washed again with sat. $NaHCO_3$ and brine and then dried over $MgSO_4$. Concentration under vacuum afforded a brown oil which was purified by column chromatography (1:9 EtOAc/pet. ether). The solvent was removed to afford the title compound as a clear colourless oil which slowly crystallised to a white solid (0.232g, 78%) ^{1}H NMR (400 MHz, Chloroform-*d*) δ 7.93 (d, *J* = 8.5 Hz, 1H), 7.76 (d, *J* = 8.6 Hz, 1H), 7.47 (d, *J* = 8.6 Hz, 1H), 7.43 (s, 2H), 7.41 (d, *J* = 8.1 Hz, 1H), 4.57 (s, 2H), 2.49 (s, 2H). ^{13}C NMR (101 MHz, $CDCl_3$) δ 191.11, 146.92, 141.85, 141.23, 141.10, 137.16, 133.81, 132.31, 131.07, 130.36, 129.58, 128.25, 127.20, 44.13, 21.97.

(4-(Bromomethyl)-2,6-dichlorophenyl)(4'-chlorophenyl)methanone (41)

To a solution of **SJM-169-291/293** (0.23 g, 0.74 mmol) in anhydrous THF (2 mL), under a nitrogen atmosphere, phosphorus tribromide (76.3 µL, 0.81 mmol) was added. The mixture was stirred at room temperature for 2 hours and then quenched with sat. $NaHCO_{3(aq)}$ and extracted into diethyl ether twice. The combined organic phases were washed with brine and then dried over $MgSO_4$. The solvent was removed under vacuum to afford a white solid which was purified by preparative TLC (5:95 EtOAc/pet. ether) (0.138 g, 49%). ^{1}H NMR (400 MHz, Chloroform-*d*) δ 7.76 (d, *J* = 8.6 Hz, 1H), 7.47 (d, *J* = 8.6 Hz, 1H), 7.42 (s, 1H), 4.43 (s, 1H). ^{13}C NMR (101 MHz, $CDCl_3$) δ 191.09, 141.44, 141.24, 137.16, 133.81, 132.29, 131.08, 129.58, 128.79, 30.42. LCMS; t_R = 3.20min. HRMS (ESI-TOF) *m/z* calc. for $C_{14}H_8$ $BrCl_3O$ $[M+H]^+$; 376.8897 found; 376.8892 and 398.8716 $[M+Na]^+$.

5-Amino-1-(4[4-chlorobenzoyl]-3,5-dichlorobenzyl)-imidazole-4-carboxamide formate (12)

To 5-amino-1*H*-imidazole-4-carboxamide (0.045g, 0.36 mmol) in DMF (2 mL) at 0°C under a nitrogen atmosphere, sodium hydride (60% in mineral oil, 14.3 mg, 0.36 mmol) was added. The mixture was allowed to warm to room temperature and was stirred for 1.25 hours. After this time **41** (0.135 g, 0.36 mmol) in DMF (1 mL) was added dropwise and the reaction mixture was stirred for 3.5 hours.

The reaction was quenched with water and extracted with ethyl acetate. The organic layer was washed with water and brine and then dried over $MgSO_4$. The solvent was removed to afford a dark purple residue which was purified by column chromatography (1:9 MeOH/DCM). As a small impurity remained the lilac solid was precipitated from EtOAC/pet. ether and then further purified by semi-prep RP-HPLC (40% to 95% B over 15 mins). The title product was afforded as a white solid after lyophilisation (19.0 mg, 13%). ^{1}H NMR (400 MHz, Methanol-d_4) δ 8.46 (s, 1H), 7.77 (d, *J* = 8.6 Hz, 2H), 7.56 (d, *J* = 8.7 Hz, 2H), 7.34 (2 x s, 3H), 5.21 (s, 2H). ^{13}C NMR (101 MHz, MeOD) δ 205.02, 178.36, 142.08, 137.85, 137.41, 135.28, 133.22, 132.34, 132.12, 130.62, 128.08, 123.26, 122.31, 46.41. LCMS *m/z* calc. for $C_{18}H_{13}{}^{35}Cl_3N_4O_2$ $[MH]^+$; 423.0, found; 423.1, t_R = 2.66 min. HRMS (ESI-TOF) *m/z* calc. for $C_{18}H_{14}{}^{35}Cl_3N_4O_2$ $[M+H]^+$; 423.0177 found; 423.0178 and 444.9996 $[M+Na]^+$.

3-Amino-1-(4[4-chlorobenzoyl]-3,5-dichlorobenzyl)-pyrazole-4-carboxamide hydroformate (10) and 5-amino-1-(3,5-dichloro-4-(4-chlorobenzoyl)benzyl)-1*H*-pyrazole-4-carboxamide formate (11).

To 3-aminopyrazole-4-carboxylic acid amide (0.03 g, 0.24 mmol) in DMF (2 mL) at 0°C, sodium hydride (9.5 mg, 0.24 mmol) was added. The mixture warmed to room temperature and stirred for 1hr. **41** (0.11 g, 0.24 mmol) in DMF (1 mL) was then added dropwise at 0°C. The mixture was stirred at room temperature for 1.5hrs then heated at 90°C for 24 hrs. The reaction was quenched with water and then partitioned between water and DCM. The aqueous phase was extracted with DCM and the combined organic phases were dried over $MgSO_4$ and the solvent was removed under vacuum. The resulting yellow solid was purified by column chromatography on silica (5% MeOH in DCM to 10% MeOH in DCM) to afford the title compound as a white solid (16 mg). NMR showed two products (*N*-1 and *N*-2 isomers) so these were isolated by semi-prep HPLC (35% to 47% B over 16 mins with a 1 min hold at 42% B). The products were isolated as a white solid after lyophilisation; **10** (18.5 mg, 19 %) **11** (16.4 mg, 16 %). ^{1}H NMR (400 MHz, DMSO-d_6) **10**; δ 8.53 (s, 1H), 8.05 (s, 1H), 7.77 (d, *J* = 8.5 Hz, 2H), 7.67 (d, *J* = 8.5 Hz, 2H), 7.50 (s, 2H), 5.46 (s, 1H), 5.20 (s, 2H). ^{1}H NMR (400 MHz, DMSO-d_6) **11**; δ 8.53 (s, 1H), 7.80 – 7.71 (m, 3H), 7.67 (d, *J* = 8.7 Hz, 2H), 7.37 (s, 2H), 6.44 (s, 2H), 5.25 (s, 2H). ^{13}C NMR (101 MHz, MeOD); **10;** δ = 192.42, 170.32, 158.79, 142.55, 142.12, 135.31, 133.19, 133.00, 132.11, 130.61, 128.62, 127.43, 102.62, 54.88. ^{13}C NMR (101 MHz, MeOD); **11**; δ = 192.46, 170.32, 151.84, 146.83, 142.48, 142.10, 139.84, 137.57, 135.33, 133.00, 132.11, 130.60, 128.13, 98.26, 63.18. LCMS *m/z* calc. for $C_{18}H_{13}Cl_3N_4O_2$ $[MH]^+$; 423.0, found; 423.1, t_R = 3.18 min. HRMS (ESI-TOF) *m/z* calc. for $C_{18}H_{14}Cl_3N_4O_2$ $[M+H]^+$; 423.0177 found; 423.0179 and 444.9996 $[M+Na]^+$. Analytical HPLC; (**10**) t_R = 16.53 mins, purity = 100%, (**11**) t_R = 16.83 mins, purity = 99%.

3,5-dichloro-4-(4-chlorobenzoyl) benzyl azide (42)

To **41** (50.0 mg, 0.13 mmol) in ethanol (1 mL), sodium azide (17.2 mg, 0.26 mmol) was added. The mixture was stirred at room temperature for 1 day and then poured into water. The product was extracted into ether twice and the combined organic phases were washed with water 3 times and dried over $MgSO_4$. The solvent was removed under a stream of nitrogen and the residue (44.9 mg, 100%) was used directly in the next step without further purification.

5-amino-1-(3,5-dichloro-4-(4-chlorobenzoyl)benzyl)-1*H*-1,2,3-triazole-4-carboxamide (CAI) (9)

To 2-cyanoacetamide (14.4 mg, 0.17 mmol) in ethanol (1 mL), 30% sodium methoxide in methanol (31.8 µL, 0.17 mmol) was added. The mixture was heated at reflux for 40 minutes and after cooling slightly **42** (44.9 mg, 0.13 mmol) in ethanol (1 mL) was added. The mixture was heated at reflux for 1.5 hours and after cooling the solvent was removed under a stream of nitrogen. The crude product was purified by column chromatography (19:1 DCM/MeOH) to afford the title compound as a yellow solid (20.4 mg, 36%). ^{1}H NMR (400 MHz, Methanol-d_4) δ 7.76 (d, J = 8.6 Hz, 2H), 7.55 (d, J = 8.6 Hz, 2H), 7.37 (s, 2H), 5.49 (s, 2H). ^{13}C NMR (101 MHz, MeOD) δ 192.32, 166.86, 146.75, 142.14, 141.02, 138.00, 135.23, 133.16, 132.10, 130.62, 128.44, 123.23, 54.80. LCMS *m/z* calc. for $C_{16}H_{13}Cl_3N_5O_2$ $[MH]^+$; 424.0, found; 424.1, t_R = 2.80 min. HRMS (ESI-TOF) *m/z* calc. for $C_{17}H_{13}Cl_3N_4O_2$ $[M+H]^+$; 424.0129 found; 424.0117 and 445.9965 $[M+Na]^+$.

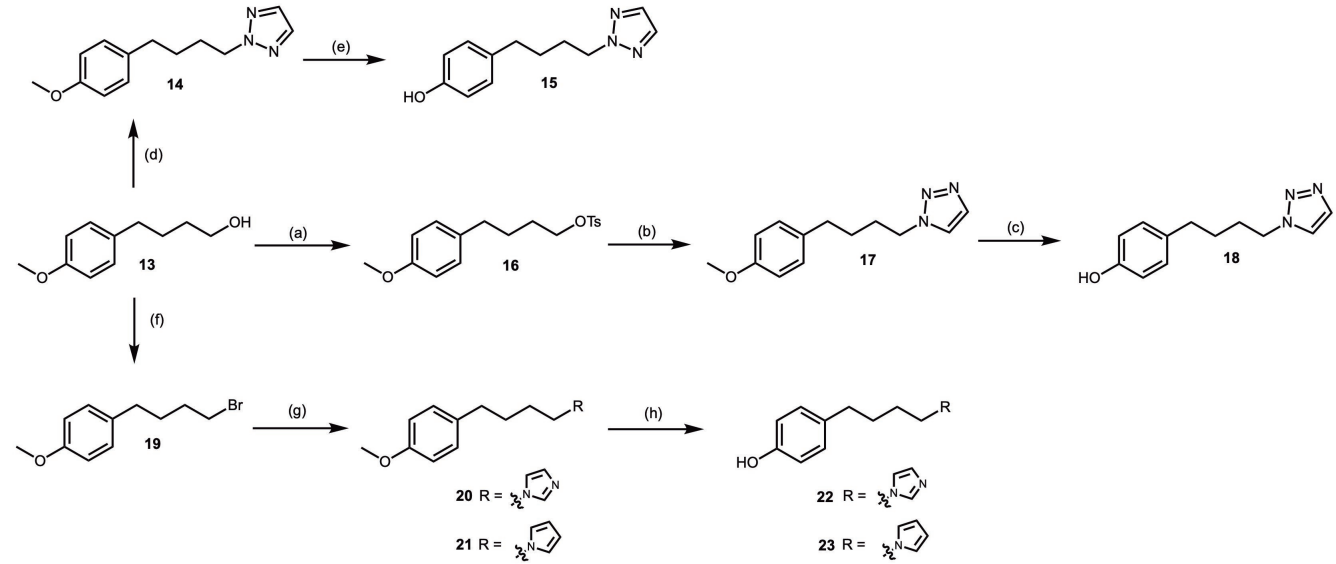

Scheme 1. *Reagents & Conditions*: (a) Tosyl chloride, triethylamine, CH_2Cl_2, 0°C → r.t., 20 h; (b) 1*H*-1,2,3-triazole, NaOH, NaI, amyl alcohol, Δ, 5h; (c) pyridine hydrochloride, MW (180 °C) 2 min then 6 min; (d) PPh_3, DIAD, 1*H*-1,2,3-triazole, THF, 19 h; (e) pyridine hydrochloride, MW (180 °C) 3 x 2 min; (f) CBr_4, PPh_3, CH_2Cl_2, 18 h; (g) Imidazole, NaH, DMF, 18 h; (h) pyridine hydrochloride, MW (180 °C) 6 min.

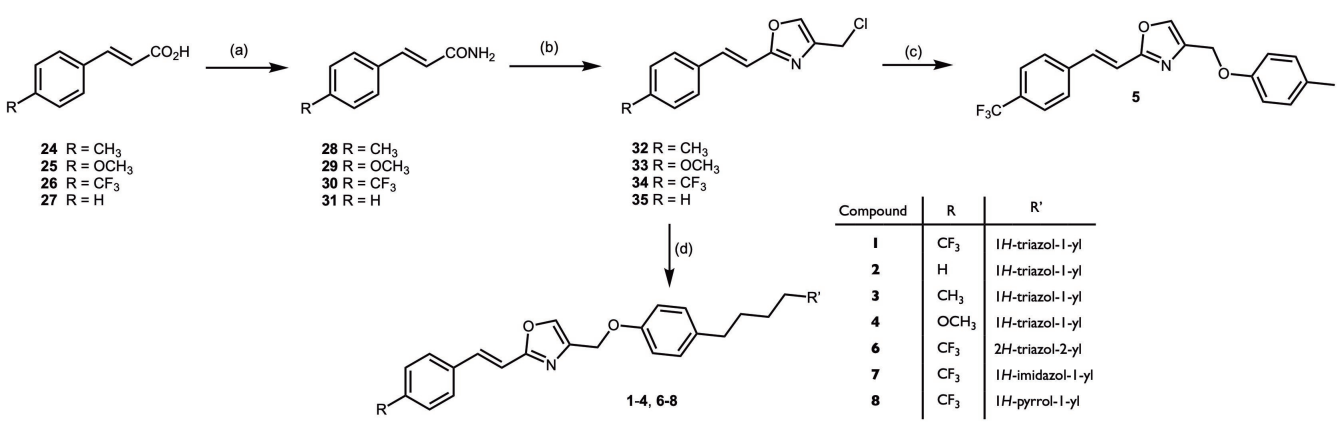

Compound	R	R'
1	CF_3	1*H*-triazol-1-yl
2	H	1*H*-triazol-1-yl
3	CH_3	1*H*-triazol-1-yl
4	OCH_3	1*H*-triazol-1-yl
6	CF_3	2*H*-triazol-2-yl
7	CF_3	1*H*-imidazol-1-yl
8	CF_3	1*H*-pyrrol-1-yl

Scheme 2. *Reagents & Conditions:* (a) (i) $(COCl_2)$, DMF, THF, (ii) NH_3, H_2O, EtOAc; (b) 1,3-dichloroacetone, toluene, Δ; (c) 4-hydroxytoluene, NaH, DMF; (d) 4-substituted phenol (cmpds **15**, **18**, **22** or **23**), NaH, DMF.

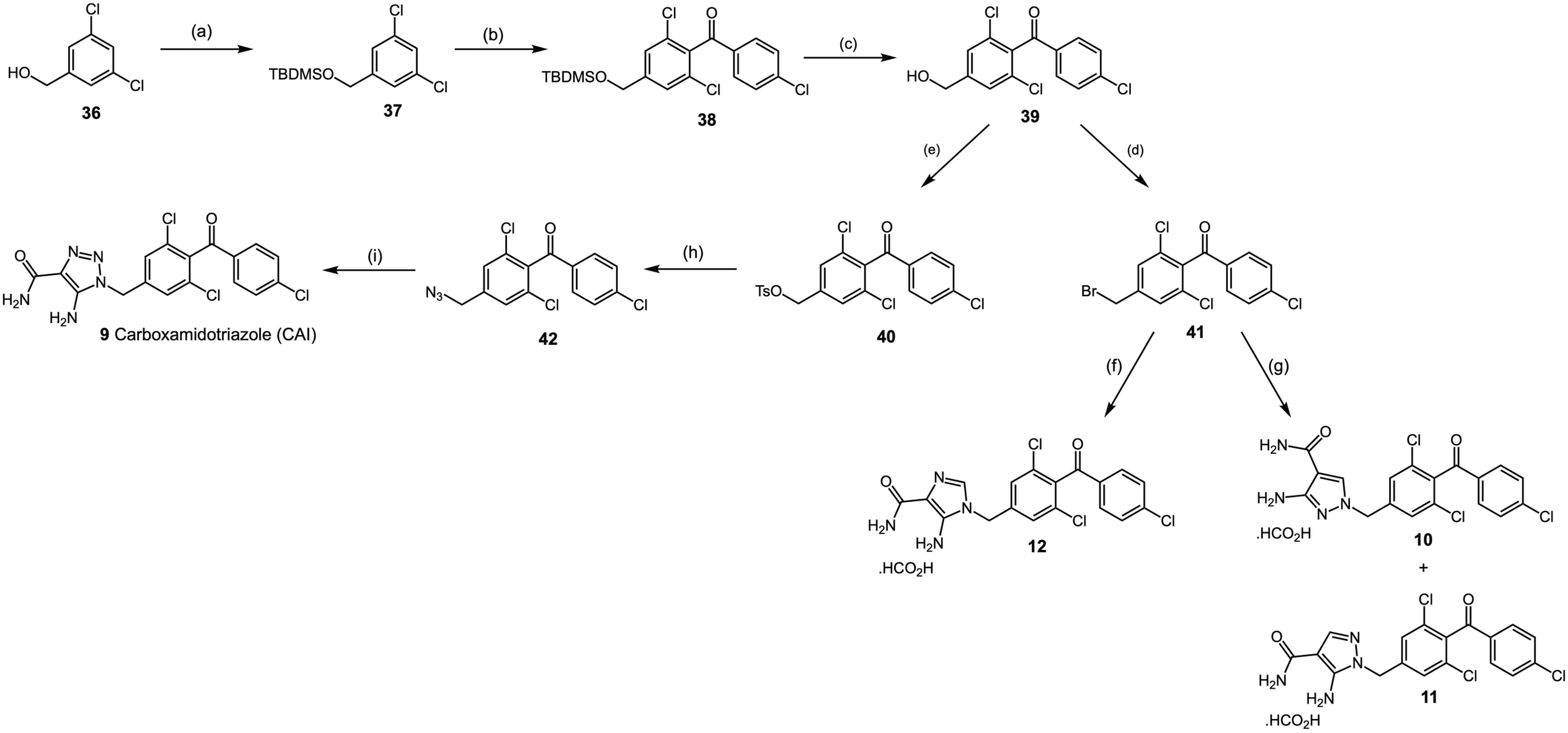

Scheme 3. *Reagents & Conditions:* (a) TBDMSCl, imidazole, DMAP, DMF; (b) (i) *n*BuLi, THF, -78 °C, 4-chlorobenzoyl chloride; (c) TBAF, THF; (d) PBr_3, THF; (e) Tosyl chloride, DIPEA, $CHCl_3$; (f) 5-amino-1*H*-imidazole-4-carboxamide, K_2CO_3, MeCN; (g) 3-aminopyrazole-carboxamide, NaH, DMF; (h) NaN_3, EtOH (i) Cyanoacetamide, EtOH, 30% NaOMe in MeOH.